

Fixed Point Hamiltonian of the Ising Model

Master thesis

Faculty of Science, University of Bern

handed in by
Wittwer Joel

2024

Supervisor
Prof. Dr. Uwe-Jens Wiese

Abstract

In this thesis, we investigate a parameterization of the fixed-point Hamiltonian for the Ising model utilizing the real space renormalization group (RSRG) technique. This method is an important approach to understand critical phenomena within statistical physics. The Ising model, a simplified framework, provides profound insights into phase transitions and critical behaviors. Initially, we discuss the concepts of renormalization group decimation and blocking in the context of the one-dimensional Ising model. Subsequently, we introduce a cluster-inspired renormalization approach. Herein, the Ising model is reformulated from its conventional spin representation to a cluster representation, characterized by active and inactive bonds among spins. Following this transformation, the model undergoes a blocking process, leading to the calculation of new Boltzmann weights for the renormalized system. We then develop a method to iterate this renormalization process and demonstrate its application through a single iteration step. In the latter part of the thesis, we present a strategy for parameterizing the two-dimensional Ising model using n -point graph functions. This approach facilitates the derivation of conditions for a finite-volume approximation of the fixed-point Hamiltonian in the two-dimensional Ising model. Using this method, we successfully identify a trivial fixed point.

Acknowledgments

I want to give a huge thank you to Prof. Dr. Uwe-Jens Wiese for all his help and guidance during my thesis work. He always made time for us, and that was priceless. Our weekly meetings were so helpful because he always had great ideas and useful suggestions that really pushed my thesis forward.

Contents

1	Introduction	6
2	Ising Model	8
2.1	Solution of the One-Dimensional Ising Model	9
2.1.1	Cluster Representation	10
2.2	Solution of the Two-Dimensional Ising Model	11
3	Monte Carlo Simulations	14
3.1	Swendsen-Wang Algorithm	15
4	Renormalisation Group	17
4.1	Renormalization of the Ising Model	17
5	Exact Renormalization Group Transformation	22
5.1	Renormalization Group Decimation	22
5.2	Renormalization Group Blocking	23
5.3	Cluster-inspired Renormalization Group	27
5.3.1	Iterations in Cluster-Inspired Renormalization	34
6	Parametrization of the Two-Dimensional Fixed Point Hamilton Function. .	38
7	Finite-Volume Approximation of the Fixed Point	40
8	Conclusion	47

1 Introduction

The Ising model [1] serves as a foundational framework within statistical physics, offering a simplified yet profound means to elucidate critical concepts. The solution of its one- and two-dimensional variants has markedly advanced the understanding of various analytical methods, such as the transfer matrix technique and series expansion [2], [3]. These solutions have furthered our understanding of critical phenomena and phase transitions. Consequently, they have enriched the discourse on the renormalization group, an innovative technique introduced by Wilson [4], [5]. The renormalization group methodology investigates the transformation of coupling constants within a system upon scaling the length. In essence, it ensures that only important couplings persist at a specific scale, thereby generating a family of Hamiltonians characterized by diverse coupling constants [6]. These Hamiltonians reside within a theory space, wherein a critical manifold exists. Atop this manifold, all theories exhibit an infinite correlation length, implying that the correlation length remain invariant under renormalization. The critical manifold harbors fixed points and acts as a basin of attraction for these points, introducing the principle of universality. This principle posits that different models sharing that they have a critical Hamiltonian on this manifold converge to a unified fixed-point Hamiltonian, thus belonging to the same universality class. Given that the Ising model undergoes a second-order phase transition, characterized by an infinite correlation length and a corresponding critical temperature, it is inferred that a fixed-point Hamiltonian exists for this model. The objective of this thesis is to identify and parameterize this Hamiltonian. To achieve this, a suitable renormalization group transformation must be selected.

To elucidate the renormalization process applied to the Ising model, an introductory exposition on the Ising model and its solutions in one and two dimensions is presented in Chapter 2. Following this, an overview of Monte Carlo techniques is provided, highlighting their necessity for the numerical solution of the Ising model. Chapter 4 delves into the renormalization group, offering a foundational discussion on renormalization principles. This includes the introduction of the blocking kernel, alongside an exploration of its implications for the partition function and observable quantities. Subsequently, the dynamics of coupling flow and the concept of fixed points are examined. In Chapter 5, an overview of established renormalization group techniques, specifically decimation [7] and block spin transformation [8], are discussed. Following this, a novel cluster-inspired renormalization group approach is introduced. This method necessitates reformulating the Ising model from its conventional spin representation to a cluster-based framework, wherein bonds between spins are classified as activated or deactivated. Subsequent steps involve calculating new Boltzmann weights for these bonds within the renormalized lattice. A methodology to iterate this process is constructed, and a single iteration is executed. However, the proliferation of distinct deactivated bond types with each renormalization cycle prevents further iterations and with that the potential to gain more insight about the fixed point.

In Chapter 6, a methodology is devised for the parametrization of the fixed-point Hamiltonian, aligning with the principles of the cluster-inspired renormalization group approach. This parametrization strategy employs n -point graphs, each assigned a specific Boltzmann weight when all spins within the graph align parallelly, and a weight of one in all other cases. Subsequently, Chapter 7 details the derivation of an analytical finite-volume approximation for the fixed-point Hamiltonian. This approximation is formulated within a finite volume, encapsulating a periodic triangular lattice comprising 12 spins. A renormalization step, characterized by a scaling factor of $\sqrt{3}$, leads to a coarser lattice structure with four spins. The spin configurations

of this coarser lattice are deduced as aggregates of various configurations from the finer lattice. By employing n -point graph parametrizations for both fine and coarse lattice configurations, a set of conditions emerges for the Boltzmann weights of the n -point graphs, facilitating the determination of the fixed-point Hamiltonian's parameters.

2 Ising Model

The Ising model, introduced by the physicist Ernst Ising in 1925, serves as a theoretical framework for understanding ferromagnetism and phase transitions. Its simplicity stems from the assumption that spin variables s_x can take on only two discrete values, ± 1 . The Ising model Hamiltonian function is given by

$$\mathcal{H}[s] = -J \sum_{\langle xy \rangle} s_x s_y - B \sum_x s_x, \quad (1)$$

where $J > 0$ represents the coupling constant for nearest-neighbor interactions, denoted by $\langle xy \rangle$, and B is an external magnetic field. Note that from now on in this thesis, the term "Hamiltonian" will refer specifically to the classical Hamiltonian function. The energy of a configuration in the Ising model depends on the alignment of adjacent spins and their interaction with the external magnetic field, reflecting the interplay between thermal fluctuations and interaction energies. In the absence of an external magnetic field ($B = 0$), the model exhibits a global \mathbb{Z}_2 symmetry under the transformation $s_x \rightarrow -s_x$ for all spins. At the critical temperature $T = T_c$, the Ising model undergoes a second-order phase transition for dimensions $d \geq 2$. For temperatures $T > T_c$, spins form several small magnetic domains of up ($s = +1$) or down ($s = -1$) orientations, whereas for $T < T_c$, spins tend to align parallel to each other. The partition function of the model is defined as

$$Z = \sum_{[s]} e^{-\beta \mathcal{H}[s]} = \prod_{x=1}^N \sum_{s_x = \pm 1} e^{-\beta \mathcal{H}[s]}, \quad (2)$$

where $\beta = 1/k_B T$, k_B is the Boltzmann constant, and T is the temperature. The two-point correlation function is given by

$$G^{(2)}(x, y) = \langle s_x s_y \rangle = \frac{1}{Z} \sum_{[s]} s_x s_y e^{-\beta \mathcal{H}[s]}. \quad (3)$$

To analyze the correlation between two sites separated by distances greater than a few lattice spacing's, it is useful to consider the connected two-point function, which subtracts the mean spin values:

$$G_c^{(2)}(x, y) = \langle s_x s_y \rangle - \langle s_x \rangle \langle s_y \rangle. \quad (4)$$

Above the critical temperature ($T > T_c$), the mean spin value approaches zero, making $G_c^{(2)}(x, y)$ and $G^{(2)}(x, y)$ equivalent. At large distances, the connected correlation function depends on the absolute distance between spins, $r = |x - y|$, and decays exponentially with distance:

$$G_c^{(2)}(x, y) \approx e^{-r/\xi}. \quad (5)$$

The correlation length ξ represents the scale over which spins are correlated. Under typical conditions, ξ does not exceed a few lattice spacings. However, at the critical temperature T_c , the correlation length diverges, indicating long-range correlations across the lattice and the emergence of universal behavior [6].

2.1 Solution of the One-Dimensional Ising Model

By considering the partition function

$$Z = \sum_{[s]} e^{-\beta\mathcal{H}[s]} \quad (6)$$

with the Hamiltonian

$$\mathcal{H}[s] = -J \sum_{\langle xy \rangle} s_x s_y - B \sum_x s_x \quad (7)$$

one can see that it is possible to rewrite the Hamiltonian as a sum over just one spin variable $x = 1, 2, \dots, N$ of the energy $E(s_x, s_{x+1})$ between two neighbor spins. Note that the energy takes only four different values, since the spins $s_x = \pm 1$ and $s_{x+1} = \pm 1$ can only take 4 values. With periodic boundary condition, the Hamiltonian can be rewritten as

$$\mathcal{H}[s] = \sum_x E(s_x, s_{x+1}) = \sum_x \left[-J s_x s_{x+1} - \frac{B}{2} (s_x + s_{x+1}) \right]. \quad (8)$$

Where J is the coupling constant of two nearest-neighbour spins and B is the external magnetic field. With this simplification it is possible to write the partition function as

$$Z = \sum_x e^{-\beta E(s_x, s_{x+1})} = \underbrace{e^{-\beta E(s_1, s_2)}}_{t_{1,2}} e^{-\beta E(s_2, s_3)} e^{-\beta E(s_3, s_4)} \dots \quad (9)$$

Where we introduced the transfer matrix $t_{s_x, s_{x+1}} = e^{-\beta E(s_x, s_{x+1})}$. With this notation one can write $e^{-\beta\mathcal{H}[s]}$ as

$$e^{-\beta\mathcal{H}[s]} = t_{s_1, s_2} t_{s_2, s_3} \dots t_{s_N, s_1}. \quad (10)$$

The components of the transfer matrix contains the Boltzmann weights of all possible spin configurations of two nearest-neighbour spins

$$t = \begin{pmatrix} e^{-\beta E(+1, +1)} & e^{-\beta E(+1, -1)} \\ e^{-\beta E(-1, +1)} & e^{-\beta E(-1, -1)} \end{pmatrix} = \begin{pmatrix} e^{\beta(J+B)} & e^{-\beta J} \\ e^{-\beta J} & e^{\beta(J-B)} \end{pmatrix}. \quad (11)$$

Now it is possible to calculate the partition function as a summation over all possible spin values over the transfer matrices

$$Z = \sum_{s_1} \sum_{s_2} \dots \sum_{s_N} t_{s_1, s_2} t_{s_2, s_3} \dots t_{s_N, s_1} = \text{Tr}[t^N] \quad (12)$$

which is the trace of the transfer matrix t to the power of the number of spins N . Since t is a real 2×2 matrix, with two orthogonal eigenstates $|\phi_{\pm}\rangle$ it is convenient to write the partition function as an function of the eigenvalues λ_{\pm} with $t|\phi_{\pm}\rangle = \lambda_{\pm}|\phi_{\pm}\rangle$.

$$Z = \langle \phi_+ | t^N | \phi_+ \rangle + \langle \phi_- | t^N | \phi_- \rangle = \lambda_+^N + \lambda_-^N, \quad \lambda_{\pm} = e^{\beta J} \left[\cosh(\beta B) \pm \sqrt{\sinh(\beta B)^2 + e^{-4\beta J}} \right] \quad (13)$$

The correlation length ξ for a given Hamiltonian $\tilde{\mathcal{H}}$, within a system situated on a lattice with lattice spacing a , is determined by the energy gap between the first two eigenvalues h_{\pm} , expressed as $a(h_- - h_+) = a/\xi$. By defining the transfer matrix $t = e^{-a\tilde{\mathcal{H}}[s]}$ and setting $\lambda_{\pm} = e^{-ah_{\pm}}$, we can compute the correlation length ξ for the one-dimensional Ising model using the equation [9]:

$$a(h_- - h_+) = \ln \left(\frac{\lambda_+}{\lambda_-} \right) = \frac{a}{\xi}. \quad (14)$$

2.1.1 Cluster Representation

For the following discussion, it is assumed that there is no external magnetic field, i.e., $B = 0$. We introduce the bond variables $b_{\langle xy \rangle} = 1, 0$. If a bond of two parallel neighboring spins is activated, the bond variable is $b_{\langle xy \rangle} = 1$; otherwise, it is zero. So we can rewrite

$$e^{-\beta E(s_x, s_y)} = \sum_{b_{\langle xy \rangle}=0}^1 e^{-\beta E(s_x, s_y, b_{\langle xy \rangle})}. \quad (15)$$

Since we have two spin values $s = \pm 1$ and two bond values, the right-hand side can take the values

$$\begin{aligned} e^{-\beta E(s, s, 1)} &= e^{\beta J} - e^{-\beta J} & e^{-\beta E(s, s, 0)} &= e^{-\beta J} \\ e^{-\beta E(s, -s, 1)} &= 0 & e^{-\beta E(s, -s, 0)} &= e^{-\beta J} \end{aligned} \quad (16)$$

such that

$$\begin{aligned} e^{-\beta E(s, s)} &= e^{\beta J} = e^{-\beta E(s, s, 1)} + e^{-\beta E(s, s, 0)} \\ e^{-\beta E(s, -s)} &= e^{-\beta J} = e^{-\beta E(s, -s, 1)} + e^{-\beta E(s, -s, 0)}. \end{aligned} \quad (17)$$

Using the bond representation, the Ising model can be reformulated to include links between neighboring spins, on these links bonds can be either active or inactive. The Boltzmann weight for an active bond is given by $W_1 = e^{\beta J} - e^{-\beta J}$, while the weight for an inactive bond is $W_0 = e^{-\beta J}$ [9]. An example of such a reformulation can be seen in Figure 1.

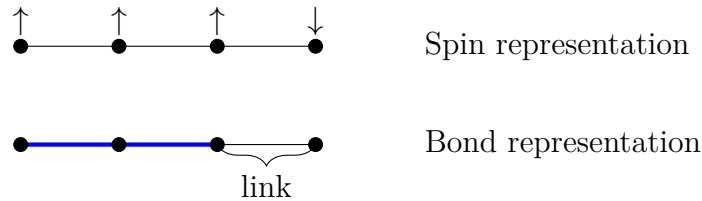


Figure 1: The Ising model has been reformulated from its spin representation to a bond representation. In this depiction, activated bonds are represented by thick blue lines, indicating the existence of an active bond between spins. Notably, there is no activated bond on the link between the second-to-last and the last spin.

This enables the expression of the Ising model's partition function in terms of the new degrees of freedom introduced by the bond variables, leading to a summation over the products of all possible bond/no-bond configurations.

$$Z = \sum_x e^{-\beta E(s_x, s_{x+1})} = \sum_x \sum_{b_{\langle x(x+1) \rangle}=0}^1 e^{-\beta E(s_x, s_{x+1}, b_{\langle x(x+1) \rangle})} = \sum_{[b]} 2^{n_c} \prod_x W_{\langle x(x+1) \rangle} \quad (18)$$

where $[b]$ denotes the summation across the products of all potential configurations of bond/no-bond weights and $W_{\langle x(x+1) \rangle}$ can take the value W_1 or W_0 whenever a bond is activated or deactivated on a link between the sites x and $x + 1$. Further n_c represents the number of clusters occurring within a configuration where clusters are defined as regions where all spins are aligned in the same direction. Spins belonging to different clusters are uncorrelated, and each spin is part of exactly one cluster. Moreover, within a cluster, all spins can be flipped

without changing the Boltzmann weight. This property allows us to express the magnetization, defined as the sum over all spins

$$M[s] = \sum_x s_x = \sum_{\mathcal{C}} M_{\mathcal{C}}, \quad (19)$$

as a sum over all clusters \mathcal{C} of the cluster magnetization $M_{\mathcal{C}}$. The cluster magnetization $M_{\mathcal{C}}$ is a sum over all spins in this cluster, and since all spins in a cluster are parallel, this sum reduces to the cluster size $|\mathcal{C}|$

$$M_{\mathcal{C}} = \sum_{x \in \mathcal{C}} s_x = \pm \sum_{x \in \mathcal{C}} 1 = \pm |\mathcal{C}|. \quad (20)$$

This also allows us to write the susceptibility χ of a d -dimensional lattice with length L as a sum over all cluster magnetisation's $M_{\mathcal{C}}$

$$\chi = \frac{1}{L^d} \langle M^2 \rangle = \frac{1}{L^d} \left\langle \left(\sum_{\mathcal{C}} M_{\mathcal{C}} \right)^2 \right\rangle = \frac{1}{L^d} \langle (M_i M_j)^2 \rangle = \frac{1}{L^d} \left\langle \sum_{i=1}^{N_{\mathcal{C}}} M_i^2 \right\rangle. \quad (21)$$

We utilized the fact that two different clusters, denoted as \mathcal{C}_i and \mathcal{C}_j , are uncorrelated for $i \neq j$. Consequently, the magnetization $M_i M_j = 0$, and only the terms where $M_i M_j = M_i^2$ for $i = j$ are non-zero and contribute to the susceptibility. By incorporating Eq. (20), the susceptibility is simplified to a sum over the cluster sizes $|\mathcal{C}|$ [9].

$$\chi = \frac{1}{L^d} \left\langle \sum_{\mathcal{C}} |\mathcal{C}|^2 \right\rangle. \quad (22)$$

2.2 Solution of the Two-Dimensional Ising Model

The solution of the two-dimensional Ising model on a square lattice was first discovered by Onsager in 1944. While the solution of the one-dimensional Ising model is relatively straightforward, the solution to the two-dimensional model is significantly more complex. In the two-dimensional Ising model, the spins are denoted by s_x , with the index x representing a node on a lattice of size L^2 . The Hamiltonian can be expressed as

$$\mathcal{H}[s] = -J \left(\sum_{\langle xy \rangle} s_x s_y + \sum_{\langle xz \rangle} s_x s_z \right) \quad (23)$$

where the external magnetic field is set to zero, $B = 0$. Similar to the one-dimensional case, the Hamiltonian for the two-dimensional Ising model can be reformulated as:

$$\mathcal{H}[s] = \sum_{i=1}^L (E(u_i, u_{i+1}) + E(u_i)), \quad E(u_i, u_{i+1}) = -J \sum_{x=1}^L s_x s_y \quad (24)$$

using the notation $u_i = \{s_1, s_2, \dots, s_L\}$ to represent the set of all spins in a column. Therefore, $E(u_i, u_{i+1})$ represents the energy between column i and its neighboring column $i+1$, and $E(u_i)$ represents the energy of column i . As in the one-dimensional model, a transfer matrix t can be defined, with elements given by

$$\langle u_i | t | u_{i+1} \rangle = e^{-\beta(E(u_i, u_{i+1}) + \frac{1}{2}E(u_i) + \frac{1}{2}E(u_{i+1}))}. \quad (25)$$

The partition function for a lattice with periodic boundary conditions is computed by taking the trace of the transfer matrix to the power of L [2]:

$$Z = \text{Tr}[t^L] \quad (26)$$

The two-dimensional Ising model exhibits two distinct phases: the low-temperature phase, where the spins are ordered, resulting in a spontaneous magnetization, and the high-temperature phase, characterized by disordered, chaotic spin behavior. The critical temperature for the phase transition in the two-dimensional Ising model on a square lattice can be determined through the duality between the partition functions of the low and high-temperature phases. The duality condition equation can be determined with the dual lattice. We introduce bond variables $\hat{b}_{\langle w, x \rangle}$, which are defined as the product of two neighboring spins s_x and s_y :

$$\hat{b}_{\langle wx \rangle} = s_x s_y = \pm 1. \quad (27)$$

Note that these bond variables are distinct from the cluster bond variables introduced in Section 2.1.1. We now define an elementary lattice square with vertices w, x, y, z , and associate four bond variables with it:

$$\hat{b}_{\langle wx \rangle} \hat{b}_{\langle xy \rangle} \hat{b}_{\langle yz \rangle} \hat{b}_{\langle zw \rangle} = s_w^2 s_x^2 s_y^2 s_z^2 = 1. \quad (28)$$

This identity holds since the spins can only take the values $s_x = \pm 1$. The constraint of eq. (28) can be reformulated using a new variable m_{\square} for each elementary lattice square:

$$\delta_{\hat{b}_{\langle wx \rangle} \hat{b}_{\langle xy \rangle} \hat{b}_{\langle yz \rangle} \hat{b}_{\langle zw \rangle} = 1} = \frac{1}{2} \sum_{m_{\square}=0}^1 \left(\hat{b}_{\langle wx \rangle} \hat{b}_{\langle xy \rangle} \hat{b}_{\langle yz \rangle} \hat{b}_{\langle zw \rangle} \right)^{m_{\square}}. \quad (29)$$

The newly introduced variable m_{\square} can be interpreted as the spin variable of the dual lattice $s_{\tilde{x}} = 1 - 2m_{\square}$, with \tilde{x} positioned at the centers of the elementary squares. The partition function

$$Z = \prod_x \sum_{s_x = \pm 1} \prod_{\langle xy \rangle} e^{\beta J s_x s_y} \quad (30)$$

can be reformulated using the newly introduced bond variables as:

$$Z = \prod_x \sum_{\hat{b}_{\langle xy \rangle} = \pm 1} \prod_{\langle wx \rangle} e^{\beta J \hat{b}_{\langle xy \rangle}} \prod_{\square} \frac{1}{2} \sum_{m_{\square}=0}^1 \left(\hat{b}_{\langle wx \rangle} \hat{b}_{\langle xy \rangle} \hat{b}_{\langle yz \rangle} \hat{b}_{\langle zw \rangle} \right)^{m_{\square}} \quad (31)$$

where \prod_{\square} denotes the product over all elementary squares. By summing over the bond variable $\hat{b}_{\langle x, y \rangle}$ on the original lattice, an interaction between the dual spins $s_{\tilde{x}}$ and $s_{\tilde{y}}$, which share the bond $\langle x, y \rangle$, is introduced:

$$\sum_{\hat{b}_{\langle xy \rangle} = \pm 1} e^{\beta J \hat{b}_{\langle xy \rangle}} \hat{b}_{\langle xy \rangle}^{m_{\square_{\tilde{x}}} + m_{\square_{\tilde{y}}}} = e^{-\tilde{\beta} \tilde{E}(s_{\tilde{x}}, s_{\tilde{y}})}. \quad (32)$$

The Hamiltonian function of the dual lattice can be defined as:

$$\tilde{\mathcal{H}}[s] = \sum_{\langle xy \rangle} \tilde{E}(s_{\tilde{x}}, s_{\tilde{y}}), \quad (33)$$

The Boltzmann factors, representing all possible combinations of two neighboring spins on the dual lattice, are calculated thus:

$$\begin{aligned} e^{-\tilde{\beta} \tilde{E}(1,1)} &= e^{-\tilde{\beta} \tilde{E}(-1,-1)} = 2 \cosh(\beta J) \\ e^{-\tilde{\beta} \tilde{E}(-1,1)} &= e^{-\tilde{\beta} \tilde{E}(1,-1)} = 2 \sinh(\beta J). \end{aligned} \quad (34)$$

By comparing the ratio of the Boltzmann factors of the original Ising model (see eq. (11)):

$$\frac{e^{-\beta E(1,-1)}}{e^{-\beta E(1,1)}} = e^{-2\beta J} \quad (35)$$

with the ratio of the dual Boltzmann factors:

$$\frac{e^{-\tilde{\beta}\tilde{E}(1,-1)}}{e^{-\tilde{\beta}\tilde{E}(1,1)}} = \tanh(\beta J), \quad (36)$$

we derive the duality condition:

$$\tanh(\beta_c J) = e^{-2\beta_c J} \quad (37)$$

where $\beta_c = 1/(k_B T_c)$. The solution for the critical inverse temperature β_c , times the coupling strength J , is then given by [6]

$$\beta_c J = \frac{1}{2} \ln(1 + \sqrt{2}). \quad (38)$$

3 Monte Carlo Simulations

By carrying out Monte Carlo simulations, one seeks to understand the time evolution of a system not through deterministic methods, such as Newtonian equations of motion, but via stochastic processes utilizing a sequence of random numbers. The results of a Monte Carlo simulation employing distinct sequences of random numbers converge within statistical errors. Within the framework of the Ising model, the Monte Carlo algorithm generates a series of spin configurations $[s^{(n)}]$, each dependent on its predecessor $[s^{(n-1)}]$. This iterative process results in a Markov chain of spin configurations:

$$[s^{(1)}] \rightarrow [s^{(2)}] \rightarrow \dots \rightarrow [s^{(N)}]. \quad (39)$$

The initial spin configuration $[s^{(1)}]$ is selected arbitrarily. Subsequent application of the algorithm for a sufficient number of iterations M allows the spin system to achieve equilibrium, which is notably independent of the initial configuration. It is critical to recognize that only configurations after the equilibration configuration, denoted as $[s^{(M)}]$, are viable for the computation of physical observables.

To estimate an observable in the simulated system, one must compute the ensemble average of its values across all configurations post-equilibration:

$$\langle \mathcal{O} \rangle = \lim_{N \rightarrow \infty} \frac{1}{N - M} \sum_{n=M+1}^N \mathcal{O}[s^{(n)}]. \quad (40)$$

In the limit $N \rightarrow \infty$, the estimation of the observable \mathcal{O} approaches its exact value. The statistical error associated with a finite number of iterations beyond equilibration, $N - M$, diminishes in proportion to $1/\sqrt{N - M}$. Consequently, to reduce the statistical error by a factor of two, the duration of the Monte Carlo simulation must be quadrupled. Two fundamental principles of Monte Carlo methods are ergodicity and detailed balance [9]. Ergodicity ensures that the Monte Carlo method is capable of accessing every possible spin configuration from any arbitrary starting point. This principle is vital for the equivalence of time averages and ensemble averages, facilitating the statistical analysis of system properties. Detailed balance states that the transition probability $p([s^{(n)}] \rightarrow [s^{(n+1)}])$ from one spin configuration to another within the Markov chain is equal to the transition probability $p([s^{(n+1)}] \rightarrow [s^{(n)}])$ for the reverse process. This can be mathematically expressed as:

$$p([s^{(n)}] \rightarrow [s^{(n+1)}]) = p([s^{(n+1)}] \rightarrow [s^{(n)}]). \quad (41)$$

The normalization condition for transition probabilities is given by:

$$\sum_{[s^{(n+1)}]} p([s^{(n)}] \rightarrow [s^{(n+1)}]) = 1. \quad (42)$$

The detailed balance condition implies that the system evolves towards a stationary state characterized by the largest eigenvalue of the transition probability matrix. Ergodicity ensures the existence of this eigenvalue, thereby guaranteeing the uniqueness of the equilibrium state [10]. To align the equilibrium distribution with the canonical Boltzmann distribution $p[s] = e^{-\beta H[s]}$, it can be demonstrated that this distribution is indeed an eigenvector of the transition probability matrix $p([s^{(n)}] \rightarrow [s^{(n+1)}])$:

$$\begin{aligned} \sum_{[s^{(n)}]} e^{-\beta \mathcal{H}[s^{(n)}]} p([s^{(n)}] \rightarrow [s^{(n+1)}]) &= \sum_{[s^{(n)}]} e^{-\beta \mathcal{H}[s^{(n+1)}]} p([s^{(n+1)}] \rightarrow [s^{(n)}]) \\ &= e^{-\beta \mathcal{H}[s^{(n+1)}]} \sum_{[s^{(n)}]} p([s^{(n+1)}] \rightarrow [s^{(n)}]) = e^{-\beta \mathcal{H}[s^{(n+1)}]}. \end{aligned} \quad (43)$$

This relationship ensures that the Monte Carlo simulation, when converged to equilibrium, reflects the statistical mechanics of the system under the Boltzmann distribution [9].

3.1 Swendsen-Wang Algorithm

The Swendsen-Wang algorithm is a cluster-flipping method proposed by Swendsen and Wang [11]. This algorithm creates clusters of aligned spins by probabilistically forming bonds between neighboring parallel spins, with the probability determined by Boltzmann factors, as outlined in Chapter 2.1.1.

The bond formation probability between two parallel spins is given by:

$$P_{\text{bond}} = \frac{e^{-\beta E(s,s,1)}}{e^{-\beta E(s,s)}} = \frac{e^{\beta J} - e^{-\beta J}}{e^{\beta J}} = 1 - e^{-2\beta J}. \quad (44)$$

The expression $e^{-\beta E(s,s,1)}$ represents the Boltzmann weight for the scenario where a bond is active between two parallel spins, while $e^{-\beta E(s,s)}$ corresponds to the overall weight when two spins are parallel. In this algorithm, spins which are connected to other spins through bonds form clusters. The procedure ensures that ultimately, each spin belongs to exactly one cluster. Each cluster is then flipped with a probability of $\frac{1}{2}$. At temperatures above the critical temperature, the probability is high that no bonds will form, leading to a completely random configuration as no clusters can form. This characteristic ensures the algorithm's ergodicity, meaning it can potentially explore all possible spin configurations.

To demonstrate detailed balance, it suffices to consider two neighboring spins. Detailed balance requires that the transition from a state with an active bond to one without must be equally probable as the reverse transition from a state with a deactivated bond to a state with an activated bond. Starting with an active bond $e^{-\beta E(s,s,1)}$, the probability that two spins remain parallel after a cluster flip is 1, since they belong to the same cluster. The probability that no bond is reformed is $1 - P_{\text{bond}}$. In the case of two initially non-bonded spins, there are two scenarios. If the spins are antiparallel $e^{-\beta E(s,-s,0)}$, the probability of them aligning after a cluster flip is $\frac{1}{2}$, followed by the formation of a bond with probability P_{bond} . For two parallel spins without an initial bond $e^{-\beta E(s,s,0)}$, the likelihood of them remaining parallel after a flip is $\frac{1}{2}$, with a subsequent P_{bond} chance of bond formation. The detailed balance condition implies:

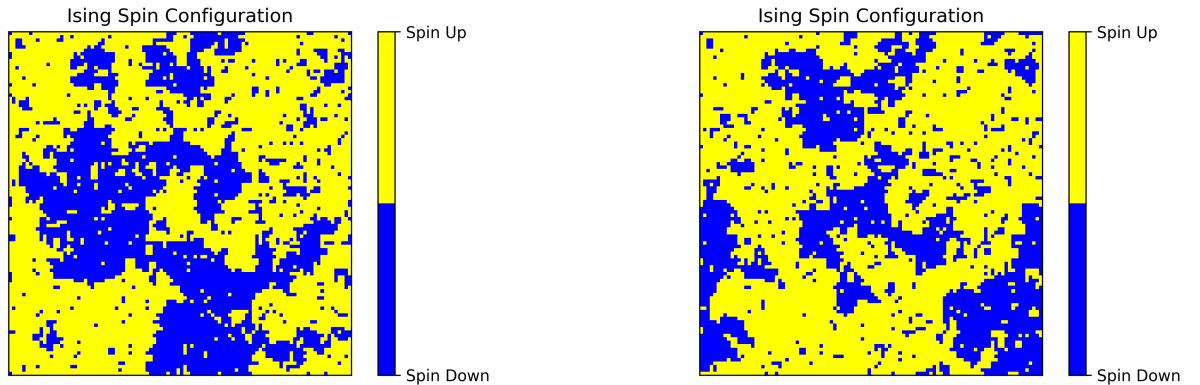
$$\begin{aligned} e^{-\beta E(s,s,1)}(1 - P_{\text{bond}}) &= e^{-\beta E(s,-s,0)}\frac{1}{2}P_{\text{bond}} + e^{-\beta E(s,s,0)}\frac{1}{2}P_{\text{bond}} \implies \\ e^{-\beta J} - e^{-3\beta J} &= e^{-\beta J} - e^{-3\beta J}. \end{aligned} \quad (45)$$

which, upon simplification, validates the detailed balance principle for the Swendsen-Wang algorithm. At high temperatures, the clusters formed tend to be small, while at low temperatures, large clusters of aligned spins emerge due to the high bond-formation probability, leading to an oscillation between similar looking spin configurations since after a cluster flip the spins tend to be again in the same cluster. Near the critical temperature T_c , a diverse range of cluster sizes are generated which leads to significant configurational changes, though that the hazard of critical slowing down is reduced. Critical slowing down refers to the phenomenon where the relaxation time, the time it takes for a system to return to equilibrium after a disturbance, increases dramatically as the system approaches a critical point of a phase transition [12]. The implementation of the Swendsen-Wang algorithm proceeds as follows:

Swendsen-Wang algorithm for the Ising model

1. Initialise a spin configuration with up (+1) and down (-1) spins.
2. Choose a spin and add all parallel neighbors with probability $P_{\text{bond}} = 1 - e^{-2\beta J}$ to the cluster.
3. Add all neighbors of the newly added spins to the cluster with probability P_{bond} .
4. Repeat step 3 until no new spins are added to the cluster.
5. Repeat steps 2 to 4 for all spins on the lattice that are not part of any cluster.
6. Once all clusters are identified, flip each cluster with a 50% probability. This means that all spins in a given cluster are flipped simultaneously, either from +1 to -1 or from -1 to +1.
7. Return to step 2

A visualization of the two-dimensional Ising model, simulated using the Swendsen-Wang algorithm on a square lattice with periodic boundary conditions, is presented in Figure 2. This figure illustrates the balance between the system's energetic interactions, represented by spin clusters, and thermal fluctuations, which is a typical behavior of the system at the critical temperature.



((a)) Spin configuration 1.

((b)) Spin configuration 2.

Figure 2: Two spin configurations generated using the Swendsen-Wang algorithm after 10,000 thermalization sweeps. The lattice size is $L = 100$, containing L^2 spins. The simulation was conducted at the critical temperature T_c .

4 Renormalisation Group

The key aspect describing the renormalization group is that it represents a continuous family of transformations of the coupling constants with a corresponding change in the length scale of the physical system. For example, if one wants to study a physical system at a certain length scale, it is convenient to consider only the degrees of freedom that are important at this length scale. This is exactly what the renormalization group does, using the transformation of the couplings. This transformation leads to a family of Hamiltonians that are associated with the degrees of freedom at a given length scale. Starting with a Hamiltonian on a critical surface at a certain length scale, for example, the lattice spacing a , and starting to rescale the system iteratively with $a \rightarrow a' = ab$, the couplings of the Hamiltonian get amplified or deamplified until the fixed-point Hamiltonian is reached, where the couplings stay constant under further iterations. If a coupling gets amplified, it is a relevant coupling; otherwise, it is an irrelevant coupling. This amplification or deamplification leads to the principle of universality, which means that, for example, two different magnets with different atoms may have the same fixed-point Hamiltonian.

The renormalization group is not a group in a mathematical sense because the transformations are not invertible but it has the property of a semi group [6].

4.1 Renormalization of the Ising Model

First, let's start with an arbitrary Hamiltonian on a d -dimensional lattice $\mathcal{H}[s_x]$, where s_x are the degrees of freedom (spins) placed at the lattice sites with lattice spacing a . The partition function of the system is given by

$$Z = \sum_{[s_x]} e^{-\mathcal{H}[s_x]}. \quad (46)$$

The renormalization group transformations are transformations that block spins s_x in given disjoint blocking areas $\Omega_{x'}$ on the lattice together and assign a new coarse spin variable $s'_{x'}$ to each area, so that these new spins are the sites of the new resulting coarse lattice. These transformations are defined through the blocking kernel $T(s_x; x \in \Omega_{x'}, s'_{x'})$, which can be interpreted as the conditional probability that the original spin s_x in the block $\Omega_{x'}$ results in the coarse spin $s'_{x'}$:

$$p(s_x | s'_{x'}, x \in \Omega_{x'}) \geq 0. \quad (47)$$

Consequently, the blocking kernel must fulfill the following equation:

$$\sum_{[s'_{x'}]} T(s_x; x \in \Omega_{x'}, s'_{x'}) = 1. \quad (48)$$

The probability for a given spin configuration is given by

$$P([s_x]) = e^{-\mathcal{H}[s_x]} \quad (49)$$

Thus, we can define the Hamiltonian of the new coarse lattice $\mathcal{H}'[s'_{x'}]$ with the probability of a given spin configuration on the original lattice and with the conditional probability from Eq. (47) as

$$e^{-\mathcal{H}'[s'_{x'}]} = \sum_{[s_x]} \prod_{\text{blocks}} T(s_x; x \in \Omega_{x'}, s'_{x'}) e^{-\mathcal{H}[s_x]}. \quad (50)$$

Through the above conditions, the partition function Z' of the coarse Hamiltonian on the coarse lattice is identical to the partition function of the original Hamiltonian.

$$Z' = \sum_{[s'_{x'}]} e^{-\mathcal{H}'[s'_{x'}]} = \sum_{[s'_{x'}]} \sum_{\{s_x\}} \prod_{\text{blocks}} T(s_x; x \in \Omega_{x'}, s'_{x'}) e^{-\mathcal{H}[s_x]} = \sum_{[s_x]} e^{-\mathcal{H}[s_x]} = Z. \quad (51)$$

The invariance of the partition function under renormalization transformations also applies to any arbitrary expectation value of a function X dependent on the spin variables s'_x . The outcome is consistent, regardless of whether the expectation value of X is calculated using the original Hamiltonian $\mathcal{H}[s_x]$ or the transformed Hamiltonian $\mathcal{H}'[s'_{x'}]$.

$$\langle X \rangle = \frac{1}{Z'} \sum_{[s'_{x'}]} X[s'_{x'}] e^{-\mathcal{H}'[s'_{x'}]} = \frac{1}{Z} \sum_{[s_x]} X[s'_{x'}] e^{-\mathcal{H}[s_x]} \quad (52)$$

There are various types of blocking kernels, which can primarily be categorized into deterministic and probabilistic types. However, in the case of the renormalization of the Ising model, they all block areas $\Omega_{x'}$ with fine spins s_x together and assign a new spin to the block $s'_{x'}$. The case of a factor b blocking, which means that the lattice spacing of the fine lattice a is transformed to a coarse lattice $a \rightarrow ab$ with $b > 1$, is represented in Figure 3.

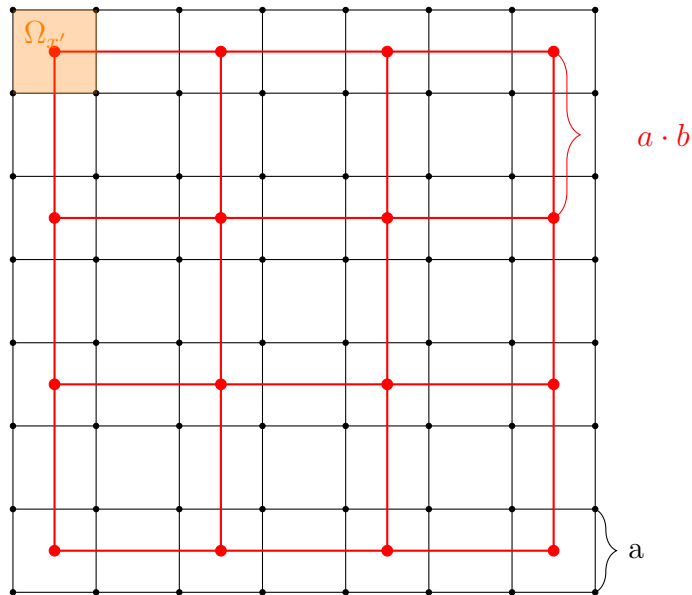


Figure 3: Original lattice with a lattice spacing a and with a blocking region $\Omega_{x'}$ of 4 spins s_x . The four spins s_x within $\Omega_{x'}$ are blocked to a coarse spin $s'_{x'}$ in the center of the block. The coarse lattice has lattice spacing $a \cdot b$ (In this case $b = 2$).

In the case of a deterministic blocking kernel, the new spin variable becomes a function of several original spin variables:

$$s'_{x'} = f(s_x), \quad x \in \Omega_{x'}. \quad (53)$$

This transformation can be repeated multiple times. If we block the original lattice n times, the equation above becomes [13]:

$$s_{x^n}^n = f(s_{x^{n-1}}^{n-1}), \quad x^{n-1} \in \Omega_{x^n}. \quad (54)$$

Two common deterministic renormalization techniques are: (i) decimation

$$s'_{x'} = s_x, \quad x \in \Omega_{x'}. \quad (55)$$

where the value of an original spin determines the coarse spin; and (ii) majority rule

$$s'_{x'} = c \sum_{x \in \Omega_{x'}} s_x. \quad (56)$$

where c is the renormalization constant, which ensures the correct value of the coarse spin $s'_{x'}$ when the number of spins s_x in a block $\Omega_{x'}$ is even [13]. Note that these transformations are irreversible, since it is not possible to determine the values of s_x by knowing just the values $s'_{x'}$.

Furthermore, there are blocking kernels which define the coarse spin $s'_{x'}$ of a blocking area probabilistically. One of them is the mostly used blocking kernel in this master thesis:

$$T(s_x; x \in \Omega_{x'}, s'_{x'}) = A + \frac{1 - 2A}{N} \sum_{x \in \Omega_{x'}} \delta_{s_x, s'_{x'}}. \quad (57)$$

where N is the number of spins s_x in the blocking area $\Omega_{x'}$, and A is the probability that the coarse spin $s'_{x'}$ is not aligned with any of the fine spins in the blocking area. Note that this blocking kernel also has the property of a semigroup so that blocking with the above kernel followed by the blocking of the form

$$T(s'_{x'}; x' \in \Omega_{x''}, s''_{x''}) = B + \frac{1 - 2B}{M} \sum_{x' \in \Omega_{x''}} \delta_{s'_{x'}, s''_{x''}} \quad (58)$$

is equivalent to the blocking kernel:

$$T(s_x; x \in \Omega_{x''}, s''_{x''}) = A' + \frac{1 - 2A'}{NM} \sum_{x \in \Omega_{x''}} \delta_{s_x, s''_{x''}} \quad (59)$$

where $A' = A + B - 2AB$. This property of the blocking kernel is extremely useful since several blocking steps can be performed in just one step. By blocking n steps in just one large step, the probability that the coarse spin $s^n_{x^n}$ is not aligned with any original spin becomes

$$A^n = \frac{1}{2} - \frac{1}{2} \prod_{i=1}^n (1 - 2A_i) \quad (60)$$

where $A = A_1$, $B = A_2$, etc., are the probabilities that no spin is aligned from the smaller blocking steps.

Starting with the Hamiltonian $\mathcal{H}[s]$ of the Ising model, which includes only nearest-neighbor interactions with coupling strength $g = \beta J$, the renormalized Hamiltonian $\mathcal{H}'[s']$ could also contain next-to-nearest neighbor interactions. Therefore, it is essential not to limit the description of the Hamiltonian to a single coupling constant, as new couplings may emerge at each renormalization step. Accordingly, we must consider the entire set of coupling constants $\{g\} = (g, g_2, \dots)$ that respect the symmetry of the model and the renormalization group (RG) process. This RG process transforms these couplings across steps $\{g\} \rightarrow \{g'\} \rightarrow \{g''\} \dots$, driving the couplings along a trajectory in their manifold. It's important to rescale the correlation length ξ with each new lattice spacing, adjusting as follows:

$$\xi(g) = \frac{\xi(g')}{b} \quad (61)$$

This trajectory can stabilize at a fixed point in the coupling space, where a renormalization transformation leaves the coupling constants unchanged, $g^* \rightarrow g^*$. At such fixed points, the correlation length behaves as:

$$\xi(g^*) = \frac{\xi(g^*)}{b} \quad (62)$$

resulting in its reduction or divergence. Fixed points are categorized into critical points, where the correlation length becomes infinite ($\xi = \infty$), and trivial points, where it reduces to zero ($\xi = 0$). Moreover, fixed points can be attractive, drawing nearby couplings towards them, or repulsive, pushing couplings away.

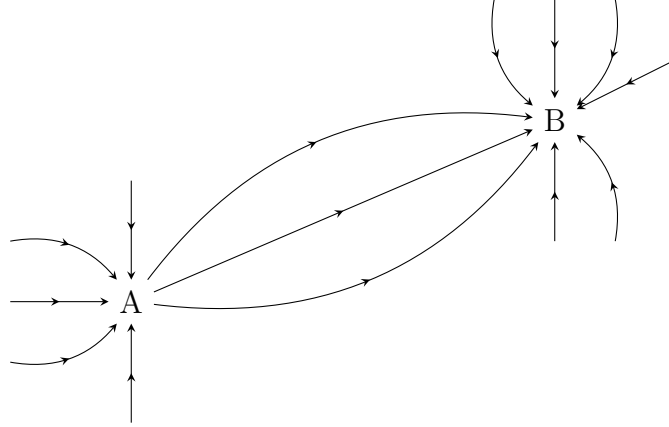


Figure 4: Two fixed points in a plane. Fixed point A represents a repulsive fixed point where the renormalization flow of the couplings (indicated with the arrow lines) points towards it, but some of it flows out of the fixed point. Fixed point B is attractive since the flow of the couplings points all to the point and nothing flows out.

In the space of coupling constants $\{g\} = (g_1, g_2, \dots)$, there exists a hypersurface C , at which the correlation length is infinite, termed the critical surface. The critical surface also acts as a basin of attraction for the critical point g^* . This implies that starting at a point on the critical surface (for example, the Ising Hamiltonian at critical temperature) and performing renormalization steps will cause the couplings to evolve within the critical surface towards the fixed point g^* .

This fixed point is notable as all theories with critical points on this surface and within the basin of attraction of g^* exhibit identical continuum physical behavior, characterized by the Hamiltonian $\mathcal{H}(g^*)$. This places them within the same universality class of Hamiltonians. Note that starting at a point that is infinitesimally outside of the critical surface and beginning to renormalize, the flow of the couplings moves away from the fixed point along the renormalized trajectories. [6] [14].

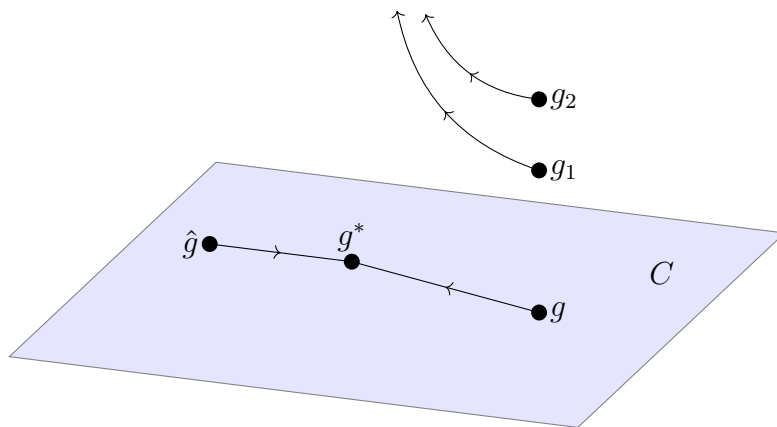
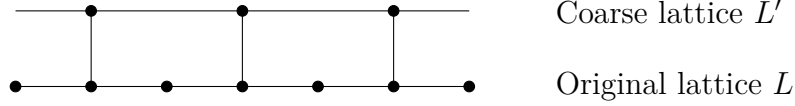


Figure 5: Consider the critical surface C in the space of coupling constants, with two points g and \hat{g} on it. Initiating the renormalization procedure at these points leads to a flow towards the fixed point g^* , which is also located on the critical surface. Points located outside of the critical surface (g_1 and g_2) will flow away from the surface under the application of renormalization steps.

5 Exact Renormalization Group Transformation

5.1 Renormalization Group Decimation

Let's begin by examining a straightforward renormalization transformation applied to the one-dimensional Ising model, known as decimation. This process involves integrating out every alternate spin on the original lattice L , resulting in the formation of a new lattice L' .



We can now proceed to compute the transfer matrix t' , previously defined in eq. (11). This computation incorporates the updated Boltzmann weights associated with the new lattice L' .

$$t' = \begin{pmatrix} e^{-\beta E'(+1,+1)} & e^{-\beta E'(+1,-1)} \\ e^{-\beta E'(-1,+1)} & e^{-\beta E'(-1,-1)} \end{pmatrix} \quad (63)$$

This matrix accounts for the various possible interactions between neighboring spins of the new lattice.

$e^{-\beta E'(+1,+1)} = e^{2\beta J} e^{\beta B} + e^{-2\beta J} e^{-\beta B} = 2 \cosh(2\beta J + \beta B)$

$e^{-\beta E'(+1,-1)} = e^{\beta J} e^{-\beta J} e^{\beta B} + e^{-\beta J} e^{\beta J} e^{-\beta B} = 2 \cosh(\beta B)$

$e^{-\beta E'(-1,-1)} = e^{-2\beta J} e^{\beta B} + e^{2\beta J} e^{-\beta B} = 2 \cosh(2\beta J - \beta B)$

(64)

We can thus identify the transfer matrix t' for the coarse lattice L' as follows:

$$t' = \begin{pmatrix} 2 \cosh(2\beta J + \beta B) & 2 \cosh(\beta B) \\ 2 \cosh(\beta B) & 2 \cosh(2\beta J - \beta B) \end{pmatrix}, \quad (65)$$

where the eigenvalues are:

$$\lambda'_{\pm} = 2 \cosh(\beta B) \cosh(2\beta J) \pm \sqrt{3 - \cosh(4\beta J) + \cosh(2\beta B) (1 + \cosh(4\beta J))}. \quad (66)$$

Since the decimation renormalization transformation integrates out every second spin of the original lattice, the correlation length of the coarse lattice ξ' must be twice as long as the original one, $\xi' = 2\xi$, and indeed this is the case:

$$\ln \left(\frac{\lambda'_-}{\lambda'_+} \right) = 2 \ln \left(\frac{\lambda_-}{\lambda_+} \right) = \ln \left(\frac{\lambda'_-}{\lambda'_+} \right) = \frac{2a}{\xi} \quad (67)$$

To derive the new coupling constant J' and the magnetic field B' , such that the transfer matrix of the coarse lattice L' (and consequently the new Hamiltonian H'), retains the same form as the original Hamiltonian H , we need to establish two equations that map $J \rightarrow J'$ and

$B \rightarrow B'$. These equations can be formulated by comparing the ratios of the transfer matrix elements of the original Ising Model with those of the renormalized system, ensuring they are represented in a consistent manner,

$$\frac{e^{-\beta E'(+1, +1)}}{e^{-\beta E'(+1, -1)}} = \frac{2 \cosh(2\beta J + \beta B)}{2 \cosh(\beta B)} \stackrel{!}{=} e^{\beta(2J' + B')},$$

$$\frac{e^{-\beta E'(-1, -1)}}{e^{-\beta E'(+1, -1)}} = \frac{2 \cosh(2\beta J - \beta B)}{2 \cosh(\beta B)} \stackrel{!}{=} e^{\beta(2J' - B')}. \quad (68)$$

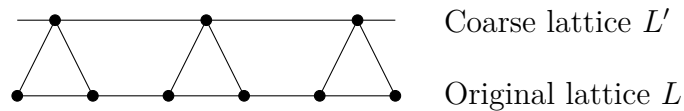
The system of eq.(68) enable us to determine the values for $\beta J'$ and $\beta B'$. By solving this equation, we can compute the renormalized coupling constants of the Hamiltonian subsequent to a single renormalization step. Furthermore, due to the semigroup property of the renormalization group, it is worth noting that by iteratively applying this equation, we can effectively simulate multiple renormalization steps, thereby exploring the system's behavior over multiple renormalization transformations,

$$\beta J' = \frac{1}{4} \ln \left(\frac{\cosh(\beta(2J - B)) \cosh(\beta(2J + B))}{\cosh(\beta B)} \right),$$

$$\beta B' = \frac{1}{2} \ln \left(\frac{\cosh(\beta(2J + B))}{\cosh(\beta B)} \right). \quad (69)$$

5.2 Renormalization Group Blocking

Next, we consider the blocking renormalization transformation. This transformation involves grouping two original spins into a single coarse-grained spin. The process is illustrated in the diagram below:



In this transformation, interactions within a block of the original lattice L and the coarse lattice L' are represented by triangles. Considering the presence of an external magnetic field B , the Boltzmann weights between the lattices can assume four different values. This variation is due to the binary nature of the original spins (up or down) and the influence of the magnetic field, which affects the Boltzmann weights differently depending on whether the coarse spin is oriented up or down.

$$\begin{array}{cccc} \uparrow \bullet & \downarrow \bullet & \downarrow \bullet & \uparrow \bullet \\ \uparrow \bullet & \uparrow \bullet & \downarrow \bullet & \downarrow \bullet \\ = x & = y & = \hat{x} & = \hat{y} \end{array} \quad (70)$$

Within the blocking triangle, there exist six distinct spin configurations, each associated with a unique Boltzmann weight. These weights depend on the Boltzmann weights of the two initial Ising spins on the fine lattice, as specified by the entries of the transfer matrix elements in eq. (11). Additionally, they depend also on the weights $A, \hat{A}, C \in [0, 1]$ which represent the likelihood that the coarse spin is not aligned with the two original spins. In the absence of an external magnetic field, it is convenient to set $A = \hat{A}$ and $C = \frac{1}{2}$.

$$\begin{array}{ccc}
 \begin{array}{c} \bullet \\ \uparrow \downarrow \\ \bullet \quad \bullet \\ \uparrow \quad \uparrow \end{array} & Ae^{\beta(J+B)} = y^2 & \begin{array}{c} \bullet \\ \uparrow \\ \bullet \quad \bullet \\ \uparrow \quad \uparrow \end{array} & (1-A)e^{\beta(J+B)} = x^2 & \begin{array}{c} \bullet \\ \downarrow \\ \bullet \quad \bullet \\ \uparrow \quad \downarrow \end{array} & Ce^{-\beta J} = y\hat{x} \\
 \begin{array}{c} \bullet \\ \uparrow \\ \bullet \quad \bullet \\ \uparrow \quad \downarrow \end{array} & (1-C)e^{-\beta J} = x\hat{y} & \begin{array}{c} \bullet \\ \downarrow \\ \bullet \quad \bullet \\ \downarrow \quad \downarrow \end{array} & \hat{A}e^{\beta(J-B)} = \hat{x}^2 & \begin{array}{c} \bullet \\ \uparrow \\ \bullet \quad \bullet \\ \downarrow \quad \downarrow \end{array} & (1-\hat{A})e^{\beta(J-B)} = \hat{y}^2
 \end{array} \tag{71}$$

Given the presence of six equations but seven parameters, C remains a free parameter, allowing the system of equations to be solved with the remaining parameters expressed as functions of C . Similar to the renormalization decimation transformation, it is possible to calculate the Boltzmann weights of two neighboring spins on the renormalized lattice,

$$\begin{array}{l}
 \begin{array}{c} \uparrow \quad \uparrow \\ \diagdown \quad \diagup \\ \bullet \quad \bullet \\ \diagup \quad \diagdown \\ \uparrow \quad \downarrow \end{array} e^{-\beta E'(+1, +1)} = x^2 e^{\beta(J+B)} + 2x\hat{y}e^{-\beta J} + \hat{y}^2 e^{\beta(J-B)} \\
 \hspace{15em} = (1-A)e^{2\beta(J+B)} + 2(1-C)e^{-2\beta J} + (1-\hat{A})e^{\beta(J-B)}, \\
 \begin{array}{c} \uparrow \quad \downarrow \\ \diagdown \quad \diagup \\ \bullet \quad \bullet \\ \diagup \quad \diagdown \\ \uparrow \quad \downarrow \end{array} e^{-\beta E'(+1, -1)} = e^{-\beta E'(-1, +1)} = xy e^{\beta(J+B)} + (y\hat{y} + x\hat{x})e^{-\beta J} + \hat{x}\hat{y}e^{\beta(J-B)} \\
 \hspace{15em} = \sqrt{A(1-A)}e^{2\beta(J+B)} + \sqrt{A(1-\hat{A})} \\
 \hspace{15em} + \sqrt{\hat{A}(1-A)} + \sqrt{\hat{A}(1-\hat{A})}e^{2\beta(J-B)}, \\
 \begin{array}{c} \downarrow \quad \downarrow \\ \diagdown \quad \diagup \\ \bullet \quad \bullet \\ \diagup \quad \diagdown \\ \downarrow \quad \downarrow \end{array} e^{-\beta E'(-1, -1)} = y^2 e^{\beta(J+B)} + 2y\hat{x}e^{-\beta J} + \hat{x}^2 e^{\beta(J-B)} \\
 \hspace{15em} = Ae^{2\beta(J+B)} + 2Ce^{-2\beta J} + \hat{A}e^{\beta(J-B)}.
 \end{array} \tag{72}$$

The probabilities A and \hat{A} are defined in terms of the parameter C as follows:

$$\begin{aligned}
 A &= \frac{1}{2}e^{-4\beta J} \left(-1 + 2C + e^{4\beta J} - \sqrt{-1 + e^{4\beta J}} \sqrt{-1 + 4C - 4C^2 + e^{4\beta J}} \right), \\
 \hat{A} &= \frac{1}{2}e^{-4\beta J} \left(-1 + 2C + e^{4\beta J} + \sqrt{-1 + e^{4\beta J}} \sqrt{-1 + 4C - 4C^2 + e^{4\beta J}} \right).
 \end{aligned} \tag{73}$$

To find the renormalized couplings J' and B' , the same process as in decimation is applied.

$$\frac{e^{-\beta E'(+1,+1)}}{e^{-\beta E'(+1,-1)}} \stackrel{!}{=} e^{\beta(2J'+B')}$$

$$\frac{e^{-\beta E'(-1,-1)}}{e^{-\beta E'(+1,-1)}} \stackrel{!}{=} e^{\beta(2J'-B')} \quad (74)$$

Once the equations are solved for J' and B' , the solution can be iteratively applied to observe the evolution of the coupling constants J and B at each stage of the renormalization process, as illustrated in Figure 6. The chosen renormalization transformation involves a factor-two blocking, implying that the lattice spacing of the coarse lattice is $2a$ if the original lattice spacing is a . Consequently, the correlation length ξ is effectively halved, transforming as $\xi/a \rightarrow \xi/(2a)$, after each renormalization step. As shown in Figure 6, the coupling constant βJ approaches zero after a sufficient number of renormalization steps. In contrast, the behavior of the coupling constant βB varies, influenced by the parameter C .

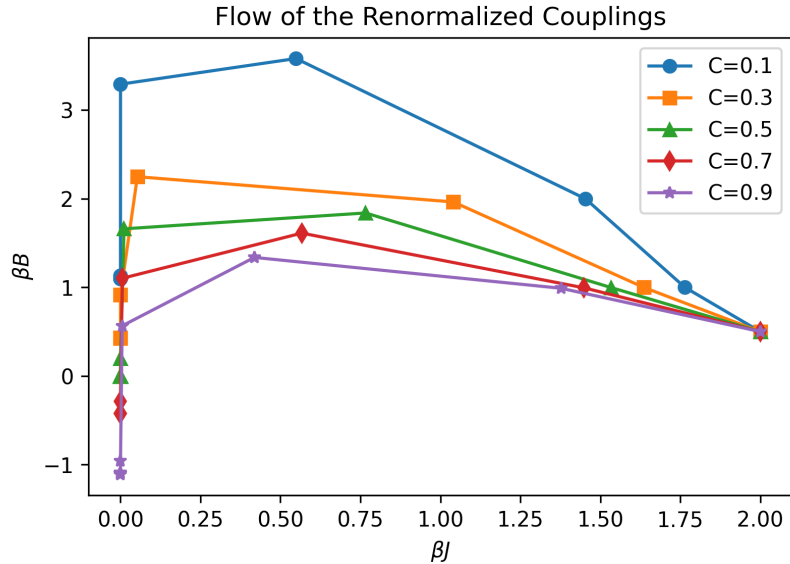


Figure 6: Flow of the couplings βJ and βB for different values of C and with starting points $\beta J = 2$ and $\beta B = 1$.

Next, we consider the blocking renormalization transformations in the absence of an external magnetic field, i.e., $B = 0$. As mentioned before, this condition simplifies the triangular blocking Boltzmann weights, making it natural to set $A = \hat{A}$ and $C = \frac{1}{2}$. Consequently, we obtain a general blocking kernel of the form :

$$T(s_x; x \in \Omega_{x'}, s'_{x'}) = A + \frac{1 - 2A}{N} \sum_{x \in \Omega_{x'}} \delta_{s_x, s'_{x'}} \quad (75)$$

In this blocking transformation, the variable N , denoting the total number of original spins within a renormalization block, is set to $N = 2$. Without an external magnetic field, the Boltzmann weights for interactions between spins on the original and the coarse lattice are characterized by just two distinct values. These weights differ, based on whether the spins from the original and coarse lattices are parallel or not,

$$\begin{array}{c} \bullet \\ \nearrow \\ \uparrow \bullet \end{array} = x, \quad \begin{array}{c} \bullet \\ \nearrow \\ \downarrow \bullet \end{array} = y. \quad (76)$$

With these simplifications, the blocking weights can be reduced to just three different cases:

$$\begin{array}{c} \bullet \\ \downarrow \\ \uparrow \bullet \quad \bullet \end{array} A e^{\beta J} = y^2, \quad \begin{array}{c} \bullet \\ \uparrow \\ \uparrow \bullet \quad \bullet \end{array} (1-A) e^{\beta J} = x^2, \quad \begin{array}{c} \bullet \\ \downarrow \\ \uparrow \bullet \quad \bullet \end{array} \frac{1}{2} e^{-\beta J} = xy \quad (77)$$

Again we factorized the Boltzmann weights of the original lattice with the probability that the coarse spin is not parallel to the two fine spins, into 2-spin interactions x, y between the fine and the coarse lattice. By solving this system of equations one finds a simple solution for A as a function of the coupling βJ

$$A = \frac{1}{2} - \frac{1}{2} \sqrt{1 - e^{-4\beta J}}. \quad (78)$$

In the renormalized system, the Boltzmann weights are simplified to just two independent scenarios: one where the two renormalized spins are parallel, and another where they are antiparallel.

$$\begin{array}{c} \uparrow \bullet \quad \bullet \uparrow \\ \diagdown \quad \diagup \\ \bullet \quad \bullet \\ \diagup \quad \diagdown \\ \uparrow \bullet \quad \bullet \downarrow \end{array} e^{-\beta E'(+1,+1)} = e^{-\beta E'(-1,-1)} = (x^2 + y^2) e^{\beta J} + 2xy e^{-\beta J} \\ = e^{-2\beta J} + e^{2\beta J} = 2 \cosh(2\beta J), \\ \begin{array}{c} \uparrow \bullet \quad \bullet \downarrow \\ \diagdown \quad \diagup \\ \bullet \quad \bullet \\ \diagup \quad \diagdown \\ \uparrow \bullet \quad \bullet \downarrow \end{array} e^{-\beta E'(+1,-1)} = e^{-\beta E'(-1,+1)} = 2xy e^{\beta J} + (x^2 + y^2) e^{-\beta J} \\ = 2. \quad (79)$$

The renormalization group blocking approach, utilizing the blocking kernel defined in eq.(75), yields renormalized Boltzmann weights identical to those obtained through renormalization group decimation, as outlined in eq.(65), for a vanishing magnetic field $B = 0$. The evolution of the coupling constant J after each renormalization step can be calculated using the following equation:

$$\frac{e^{-\beta E'(+1,+1)}}{e^{-\beta E'(+1,-1)}} = \cosh(2\beta J) \stackrel{!}{=} e^{2\beta J'} \quad (80)$$

To determine the fixed point of the recursive equation, one must examine the equation $\cosh(2\beta J^*) = e^{2\beta J^*}$. This equation has two solutions:

$$\beta J^* = 0 \quad (\text{for } T = \infty) \quad \text{and} \quad \beta J^* \rightarrow \infty \quad (\text{for } T = 0). \quad (81)$$

As illustrated in Figure 7, the coupling βJ flows to the fixed point $\beta J^* = 0$. This indicates that the system evolves towards a free theory with no interactions between spins. Consequently,

no ordered state emerges for any finite value of βJ , leading to the absence of a phase transition. Only in the limit $\beta J = \infty$, corresponding to a finite interaction coupling J at $T = 0$, do the spins exhibit order.

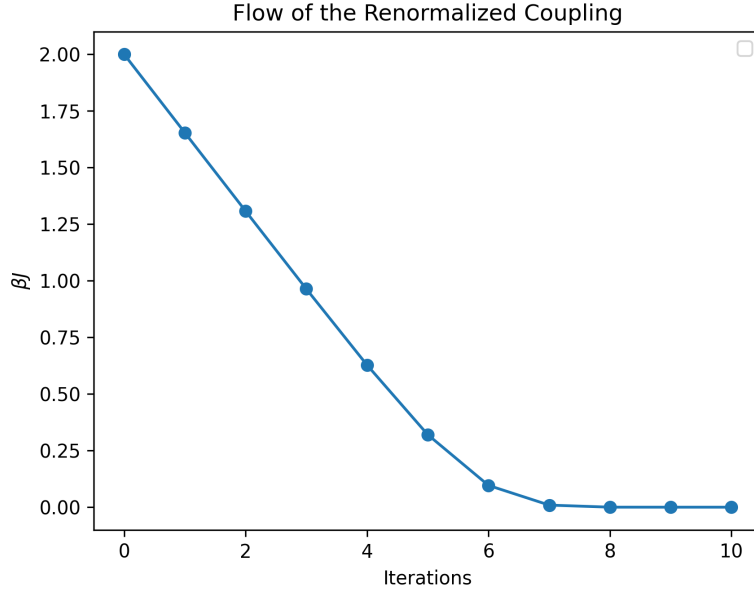


Figure 7: Flow of the coupling constant βJ after several iteration steps, as described by eq. (81), starting from $\beta J = 2$.

5.3 Cluster-inspired Renormalization Group

In this chapter, a cluster-inspired renormalization transformation applied to the one-dimensional Ising model in the absence of an external magnetic field ($B = 0$) is discussed. This transformation is applied to the original lattice, denoted by L , where the Ising model is represented through clusters as outlined in Chapter 2.1.1. With the cluster blocking kernel $T(s_x; x \in \Omega_{x'}, s'_{x'})$, we establish bonds between the lattices after renormalization, enabling the formation of spin clusters that span not only the original lattice but also the renormalized counterparts (L', L'', \dots). The geometric constructs resulting from these cluster-inspired transformations are shown in Figure 8.

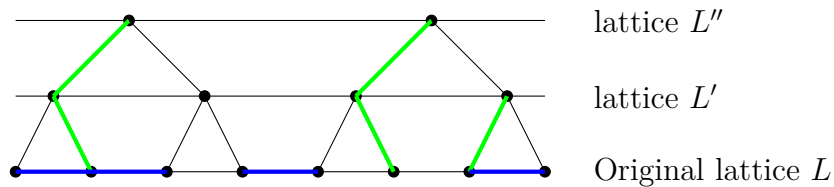


Figure 8: Geometry of the cluster-inspired renormalization group. The thick green (gray) lines represent kernel bonds that span through the renormalized lattices and the blue (black) thick lines represent the Ising-bonds between spins on the original lattice.

Initially, we must specify the allowed bonds within the blocking kernel $T(s_x; x \in \Omega_{x'}, s'_{x'})$. By examining the structure of a single renormalization block, which forms a triangle with two

fine spins and one coarse spin, it becomes apparent that we should consider various scenarios for the presence of a bond of the blocking kernel within the renormalization triangle. These scenarios, along with their respective Boltzmann weights, are outlined below.

$$\begin{array}{ccc}
 \triangle = A & \triangle = B & \triangle = C \\
 \triangle = D & \triangle = E & \triangle = F
 \end{array} \quad (82)$$

Figure 9: Representation of all possible blocking kernels using blocking triangles, where the green (gray) thick line indicates a kernel-bond between two parallel spins. The parameters $(A, B, C, D, E, F) \in [0, 1]$ denote the corresponding weights for each blocking kernel.

The blocking kernel $T(s_x; x \in \Omega_{x'}, s'_{x'})$ must satisfy the conditions $T(\uparrow\uparrow, \downarrow) + T(\uparrow\uparrow, \uparrow) = 1$ and $T(\uparrow\downarrow, \downarrow) + T(\uparrow\downarrow, \uparrow) = 1$, where the arrows represent the spin orientations. In the scenario where the fine spins are aligned upwards and the coarse spin is directed downwards, denoted as $T(\uparrow\uparrow, \downarrow)$, the weights A and C are assigned to this configuration. This allocation is justified because a bond can only be established between parallel spins. Since the fine spins are parallel, a kernel bond may or may not be established; however, since the coarse spin is antiparallel to the fine spins, no bond between them can be formed. Similar considerations lead to the following equations:

$$\begin{aligned}
 T(\uparrow\uparrow, \downarrow) + T(\uparrow\uparrow, \uparrow) &= 2(A + B + C + D) + E + F = 1 \\
 T(\uparrow\downarrow, \downarrow) + T(\uparrow\downarrow, \uparrow) &= 2(A + B) = 1
 \end{aligned} \quad (83)$$

Solving the second equation yields $B = \frac{1}{2} - A$, which implies $1 + 2(C + D) + E + F = 1$. This implies that $C = D = E = F = 0$, given that $A, B, C, D, E, F \in [0, 1]$. Bonds between spins, implied through the blocking kernel, are therefore only permitted between one fine spin and one coarse spin with the corresponding weight $\frac{1}{2} - A$. In the scenario where no kernel bonds are formed, the Boltzmann weight assigned is A . If A were set to zero ($A = 0$), there would always be activated bonds between renormalized lattices. With the various weights of the allowed blocking kernel $T(s_i, s'_i)$ defined, it is possible to determine the Boltzmann weights of the blocking triangle. These weights are constructed from the blocking kernel weight A and the weights of the Ising model on the original lattice, W_1 and W_0 . Here, W_1 represents the weight when a bond is active between two parallel neighboring spins, given by $W_1 = e^{\beta J} - e^{-\beta J}$, and W_0 is the Boltzmann weight when no bond is active, given by $W_0 = e^{-\beta J}$ as discussed in Section 2.1.1.

$$\begin{array}{ccc}
 \begin{array}{c} \bullet \\ \diagup \quad \diagdown \\ \bullet \quad \bullet \end{array} & G_1 = 2W_0 \left(\frac{1}{2} - A \right) & \begin{array}{c} \bullet \\ \diagup \quad \diagdown \\ \bullet \quad \bullet \end{array} & G_2 = 2W_0 \left(\frac{1}{2} - A \right) & \begin{array}{c} \bullet \\ \diagup \quad \diagdown \\ \bullet \quad \bullet \end{array} & G_3 = W_1 \left(\frac{1}{2} - A \right) \\
 \begin{array}{c} \bullet \\ \diagup \quad \diagdown \\ \bullet \quad \bullet \end{array} & G_4 = W_1 \left(\frac{1}{2} - A \right) & \begin{array}{c} \bullet \\ \diagup \quad \diagdown \\ \bullet \quad \bullet \end{array} & G_5 = 2W_1 A & \begin{array}{c} \bullet \\ \diagup \quad \diagdown \\ \bullet \quad \bullet \end{array} & G_6 = 4W_0 A
 \end{array} \tag{84}$$

Figure 10: Boltzmann weights of all possible combinations within a blocking area of the cluster-inspired renormalization. The green (gray) thick lines represent the kernel-bonds, and the blue (black) thick lines represent the Ising-bonds between spins.

With the Boltzmann weights from Figure 10, it is now possible to calculate the Boltzmann weight W'_1 for when a bond is formed on the renormalized lattice L' . This weight can be derived from all possible combinations of the weights from the triangular blocking areas represented in Figure 10 and the Ising-bonds between two neighboring triangles. Note that a bond on the renormalized lattice is active if the two corresponding spins are in the same cluster, connected through both the kernel and Ising-bonds. One such combination is depicted in Figure 11.

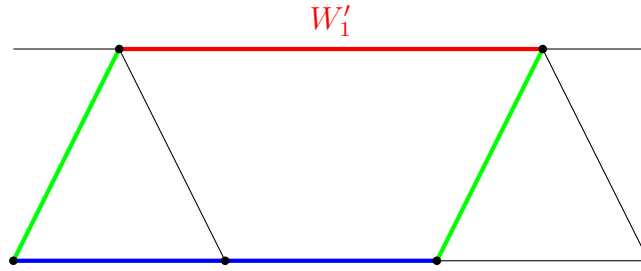


Figure 11: Possible configuration that leads to a bond W'_1 between two neighboring spins on the renormalized lattice

To generate all possible combinations that form a bond on the renormalized lattice, the approach of a transfer matrix, M_{all} , is implemented. The entries of this matrix contains the weights of all possible configurations of the triangular blocking areas of eq.(84). It is important to note that the Boltzmann weight of a blocking triangle always contributes to two bonds, as illustrated in Figure 12. Consequently, one must take the square root of the Boltzmann weights of the triangles.

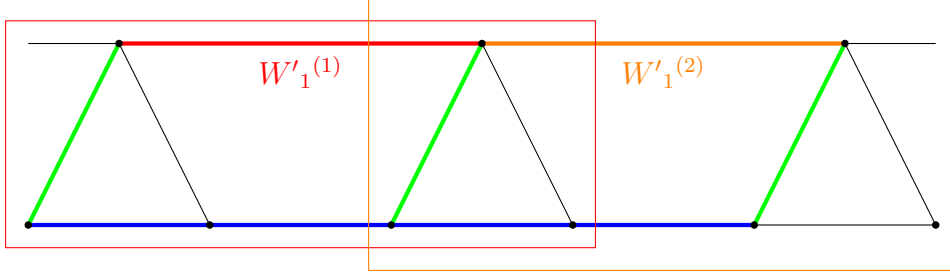


Figure 12: A chain consisting of two bonds, $W'_1(1)$ and $W_1(1)$, featuring an overlapping blocking triangle at the center.

The entries of the transfer matrix M_{all} can be calculated using the following formula:

$$M_{\text{all}ij} = \sqrt{G_i G_j}. \quad (85)$$

To construct the transfer matrix M_b , which contains only combinations of blocking areas that lead to a bond on the renormalized lattice, all other combinations must be set to zero.

$$M_b = \begin{bmatrix} 0 & 0 & 0 & 0 & 0 & 0 \\ 2W_1 \left(\frac{1}{2} - A\right) & 0 & \sqrt{2W_1 W_0} \left(\frac{1}{2} - A\right) & \sqrt{2W_1 W_0} \left(\frac{1}{2} - A\right) & 0 & 0 \\ \sqrt{2W_1 W_0} \left(\frac{1}{2} - A\right) & 0 & W_1 \left(\frac{1}{2} - A\right) & W_1 \left(\frac{1}{2} - A\right) & 0 & 0 \\ \sqrt{2W_1 W_0} \left(\frac{1}{2} - A\right) & 0 & W_1 \left(\frac{1}{2} - A\right) & W_1 \left(\frac{1}{2} - A\right) & 0 & 0 \\ 0 & 0 & 0 & 0 & 0 & 0 \\ 0 & 0 & 0 & 0 & 0 & 0 \end{bmatrix} \quad (86)$$

The Boltzmann weight for a bond of the renormalized system can be calculated with the transfer matrix and with the weight that the two blocking triangles are connected with an Ising-bond W_1 .

$$W'_1 = W_1 M_b \quad (87)$$

Similarly, we can determine the transfer matrix M_{nb} , which represents the scenario where no bond is formed between two spins on the coarse lattice.

$$M_{\text{nb}} = \begin{bmatrix} 2\left(\frac{1}{2} - A\right) W_0 & 2\left(\frac{1}{2} - A\right) W_0 & \left(\frac{1}{2} - A\right) \sqrt{2W_1 W_0} & \left(\frac{1}{2} - A\right) \sqrt{2W_1 W_0} & 2\sqrt{\left(\frac{1}{2} - A\right) W_0 A W_1} & 2\sqrt{2\left(\frac{1}{2} - A\right) A W_0} \\ 0 & 2\left(\frac{1}{2} - A\right) W_0 & 0 & 0 & 2\sqrt{\left(\frac{1}{2} - A\right) W_0 A W_1} & 2\sqrt{2\left(\frac{1}{2} - A\right) A W_0} \\ 0 & \left(\frac{1}{2} - A\right) \sqrt{2W_1 W_0} & 0 & 0 & \sqrt{2\left(\frac{1}{2} - A\right) A W_1} & 2\sqrt{\left(\frac{1}{2} - A\right) A W_0 W_1} \\ 0 & \left(\frac{1}{2} - A\right) \sqrt{2W_1 W_0} & 0 & 0 & \sqrt{2\left(\frac{1}{2} - A\right) A W_1} & 2\sqrt{\left(\frac{1}{2} - A\right) A W_0 W_1} \\ 2\sqrt{\left(\frac{1}{2} - A\right) W_0 A W_1} & 2\sqrt{\left(\frac{1}{2} - A\right) W_0 A W_1} & \sqrt{2\left(\frac{1}{2} - A\right) A W_1} & \sqrt{2\left(\frac{1}{2} - A\right) A W_1} & 2A W_1 & 2A\sqrt{2W_0 W_1} \\ 2\sqrt{2\left(\frac{1}{2} - A\right) A W_0} & 2\sqrt{2\left(\frac{1}{2} - A\right) A W_0} & 2\sqrt{\left(\frac{1}{2} - A\right) A W_0 W_1} & 2\sqrt{\left(\frac{1}{2} - A\right) A W_0 W_1} & 2A\sqrt{W_0 W_1} & 4A W_0 \end{bmatrix} \quad (88)$$

The final Boltzmann weight in the absence of activated bonds is given by:

$$W'_0 = W_0 M_{\text{all}} + \frac{W_1}{2} M_{\text{nb}} \quad (89)$$

Where W_0 is the Boltzmann weight if no Ising-bond is active and the matrix M_{all} contains all combinations of the triangular blocking weights. In order to calculate the partition function

$$M_{\text{sl}} = \begin{pmatrix} 0 & 0 & 0 & 0 & 0 & 0 \\ 0 & 0 & 0 & 0 & \sqrt{2\left(\frac{1}{2} - A\right)} W_0 & 0 \\ 0 & 0 & 0 & 0 & \sqrt{\left(\frac{1}{2} - A\right)} W_1 & 0 \\ 0 & 0 & 0 & 0 & \sqrt{\left(\frac{1}{2} - A\right)} W_1 & 0 \\ 0 & 0 & 0 & 0 & 0 & 0 \\ 0 & 0 & 0 & 0 & 0 & 0 \end{pmatrix}, \quad (92)$$

$$M_{\text{sr}} = \begin{pmatrix} 0 & 0 & 0 & 0 & 0 & 0 & 0 \\ 0 & 0 & 0 & 0 & 0 & 0 & 0 \\ 0 & 0 & 0 & 0 & 0 & 0 & 0 \\ 0 & 0 & 0 & 0 & 0 & 0 & 0 \\ \sqrt{2\left(\frac{1}{2} - A\right)} W_0 & 0 & \sqrt{\left(\frac{1}{2} - A\right)} W_1 & \sqrt{2}\sqrt{\left(\frac{1}{2} - A\right)} W_1 & 0 & 0 \\ 0 & 0 & 0 & 0 & 0 & 0 \end{pmatrix}. \quad (93)$$

However, super-bonds introduce complications due to their non-local nature, necessitating consideration of a scalar weight for every potential spin connection across the lattice. To simplify, we set $A = 0$, eliminating super-bonds ($W'_{\text{sb}} = 0$) and reducing the complexity of the $W'_{0,1}$ matrices from 6×6 to 4×4 . To ascertain the scalar Boltzmann weights $\hat{W}'_{0,1}$, we examine the transfer matrices and their diagonalization. First we see that the W'_1 matrix has one non-zero eigenvalue and W'_0 has two non-zero eigenvalues. This enables us to express the occurrence of n bonded interactions and m non-bonded interactions on the renormalized lattice as:

$$\begin{aligned} W_1^m &= S_1 D_1^n S_1^{-1} \\ W_0^m &= S_0 D_0^m S_0^{-1} = S_0 (D_0^{(1)} + D_0^{(2)})^m S_0^{-1} = S_0 D_0^{(1)m} S_0^{-1} + S_0 D_0^{(2)m} S_0^{-1} \end{aligned} \quad (94)$$

where D_1 and D_0 are diagonal matrices with the corresponding eigenvalues on the diagonal. Since W'_0 has two eigenvalues, the diagonal matrix can be split and written as $D_0 = (D_0^{(1)} + D_0^{(2)})$. Note that $D_0^{(1)} D_0^{(2)} = 0$ since both of these matrices have just one entry on the diagonal and not at the same position. The $S_{1,0}$ is the matrix that contains the eigenvectors and diagonalizes the corresponding transfer matrix $W'_{0,1}$ so that $S^{-1} W S = D$. If a non-activated bond follows an activated bond, we get a contribution from $D_0^{(1)}$ and $D_0^{(2)}$ to the whole configuration.

$$W'_1 W'_0 = S_1 D_1 S_1^{-1} S_0 D_0^{(1)} S_0^{-1} + S_1 D_1 S_1^{-1} S_0 D_0^{(2)} S_0^{-1} \quad (95)$$

To emphasise this relationship, we consider two distinct types of deactivated bonds, labeled as type (1) and type (2). The transition from an activated bond to either type of deactivated bond is characterized by distinct scalar Boltzmann weights, denoted as $\hat{W}'_0^{(1),(2)}$. These weights are directly related to the eigenvalues of their corresponding diagonal matrices, as outlined below:

$$\begin{aligned} \hat{W}'_1^n &= (-2 + e^{-2J} + e^{2J})^n, \\ \hat{W}'_0{}^{(1)m} &= \left(1 + \frac{1}{2} e^{-4J} \sqrt{e^{4J} + 3e^{8J}}\right)^m, \\ \hat{W}'_0{}^{(2)m} &= \left(1 - \frac{1}{2} e^{-4J} \sqrt{e^{4J} + 3e^{8J}}\right)^m. \end{aligned} \quad (96)$$

Furthermore, transitions involving a deactivated bond following an activated bond necessitate consideration due to the interplay between the matrices $D_1 S_1^{-1} S_0 D_0^{(1)}$ and $D_1 S_1^{-1} S_0 D_0^{(2)}$. The examination of specific entries within the matrix product $S_1^{-1} S_0$ is imperative, as their interaction with $D_0^{(1)}$ and $D_0^{(2)}$ yields distinct contributions to the overall weight. These transitions are quantified by scalar weights $\hat{W}'[B \rightarrow NB^{(1),(2)}]$, where B represents an activated bond, and $NB^{(1),(2)}$ signifies a non-activated bond of either type (1) or (2):

$$\begin{aligned}\hat{W}'[B \rightarrow NB^{(1)}] &= \frac{1 - e^{2J} + e^{-10J} \sqrt{e^{20J} + 3e^{24J}}}{2 - 2e^{2J}}, \\ \hat{W}'[B \rightarrow NB^{(2)}] &= \frac{1 - e^{2J} - e^{-10J} \sqrt{e^{20J} + 3e^{24J}}}{2 - 2e^{2J}}.\end{aligned}\tag{97}$$

Conversely, the transition dynamics from a deactivated to an activated bond, facilitated by the non-commutative nature of the matrices $S_1^{-1} S_0$ and $S_0^{-1} S_1$, introduce additional weights:

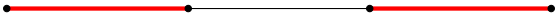
$$\begin{aligned}\hat{W}'[NB^{(1)} \rightarrow B] &= \frac{e^{10J} - e^{12J} + \sqrt{e^{20J} + 3e^{24J}}}{2\sqrt{e^{20J} + 3e^{24J}}}, \\ \hat{W}'[NB^{(2)} \rightarrow B] &= \frac{e^{12J} - e^{10J} + \sqrt{e^{20J} + 3e^{24J}}}{2\sqrt{e^{20J} + 3e^{24J}}}.\end{aligned}\tag{98}$$

In the context of a finite lattice without periodic boundary conditions, additional considerations arise for Boltzmann weights associated with boundary bonds. Specifically, activated or deactivated bonds located at the boundaries of the lattice contribute distinct weights, derived from the matrices $M_{\text{first}} S_{0,1}$ and $S_{0,1}^{-1} M_{\text{last}}$.

$$\begin{aligned}\hat{W}'[M_{\text{first}} \rightarrow NB^{(1)}] &= \frac{e^{-11J} (e^{10J} + e^{12J} - \sqrt{e^{20J} + 3e^{24J}})}{\sqrt{2}\sqrt{-e^{-J} + e^J}}, \\ \hat{W}'[M_{\text{first}} \rightarrow NB^{(2)}] &= \frac{e^{-11J} (e^{10J} + e^{12J} + \sqrt{e^{20J} + 3e^{24J}})}{\sqrt{2}\sqrt{-e^{-J} + e^J}}, \\ \hat{W}'[M_{\text{first}} \rightarrow B] &= \frac{\sqrt{2}e^{2J}\sqrt{-e^{-J} + e^J}}{-1 + e^{2J}}, \\ \hat{W}'[NB^{(1)} \rightarrow M_{\text{last}}] &= \frac{\sqrt{-e^{-J} + e^J} (e^{10J} + e^{12J} - \sqrt{e^{20J} + 3e^{24J}})}{2\sqrt{2}\sqrt{e^{20J} + 3e^{24J}}}, \\ \hat{W}'[NB^{(2)} \rightarrow M_{\text{last}}] &= \frac{\sqrt{-e^{-J} + e^J} (e^{10J} + e^{12J} + \sqrt{e^{20J} + 3e^{24J}})}{2\sqrt{2}\sqrt{e^{20J} + 3e^{24J}}}, \\ \hat{W}'[B \rightarrow M_{\text{last}}] &= \frac{e^J}{\sqrt{2}\sqrt{-e^{-J} + e^J}}.\end{aligned}\tag{99}$$

To calculate the weight of any given configuration of activated and deactivated bonds within a renormalized lattice, one can employ the scalar Boltzmann weights derived above. Consider a

specific configuration where two activated bonds are positioned at the boundaries of the lattice, with a deactivated bond of either type (1) or type (2) situated between them. The weight of such a configuration, denoted as \hat{W}'_{config} , can be expressed as the product of the weights associated with each transition and the boundary conditions.



$$\begin{aligned} \hat{W}'_{\text{config}} = & \hat{W}'[M_{\text{first}} \rightarrow B] \hat{W}'_1 \hat{W}'[B \rightarrow NB^{(1)}] \hat{W}'_0^{(1)} \hat{W}'[NB^{(1)} \rightarrow B] \hat{W}'_1 \hat{W}'[B \rightarrow M_{\text{last}}] \\ & + \hat{W}'[M_{\text{first}} \rightarrow B] \hat{W}'_1 \hat{W}'[B \rightarrow NB^{(2)}] \hat{W}'_0^{(2)} \hat{W}'[NB^{(2)} \rightarrow B] \hat{W}'_1 \hat{W}'[B \rightarrow M_{\text{last}}] \end{aligned} \quad (100)$$

where $\hat{W}'[B \rightarrow NB^{(1)}]$ represents the weight for transitioning from an activated bond to a deactivated bond of type (1), and $\hat{W}'[NB^{(1)} \rightarrow B]$ denotes the weight for transitioning from a deactivated bond of type (1) back to an activated bond. Similarly, $\hat{W}'[B \rightarrow NB^{(2)}]$ and $\hat{W}'[NB^{(2)} \rightarrow B]$ correspond to the weights for transitions involving a deactivated bond of type (2). In the above considerations, $\hat{W}'[M_{\text{first}} \rightarrow B]$ and $\hat{W}'[B \rightarrow M_{\text{last}}]$ are the weights associated with an activated bond at the boundaries. It is important to note that the boundary weights should be defined based on the specific boundary conditions and interactions at the lattice edges. This approach allows for the systematic calculation of the weights for any conceivable arrangement of activated and deactivated bonds on the renormalized lattice, thereby facilitating a comprehensive analysis of the system's statistical properties. With the establishment of scalar Boltzmann weights, it is now feasible to compute the weights of any conceivable configuration of activated and deactivated bonds within the renormalized lattice. This allows for the computation of the system's partition function, denoted as Z' , in its renormalized form. The equivalence of the partition function of the renormalized system Z' to that of the original Ising model Z underscores the correctness of the renormalization procedure and the derived Boltzmann weights \hat{W}' . This equivalence, $Z' = Z$, asserts that the renormalization step retains the essential thermodynamic quantities and phase behavior of the original system, thereby validating the computed weights.

5.3.1 Iterations in Cluster-Inspired Renormalization

The subsequent question is whether an additional renormalization step can be executed utilizing the same cluster-inspired technique as in the initial step, aiming to determine the Boltzmann weights for the further renormalized lattice L'' . This necessitates the exploration of the configurations of activated and deactivated bonds of types (1) and (2) on the lattice L' . It is understood that an activated bond may precede a deactivated bond of either type (1) or type (2), and conversely. Moreover, considering the product of the diagonal matrices $D_0^{(1)}$ and $D_0^{(2)}$, corresponding to the first and second eigenvalues of a deactivated bond, is zero ($D_0^{(1)} D_0^{(2)} = 0$), it is deduced that a deactivated bond of type (1) cannot connect with a deactivated bond of type (2). This reduces the viable bond combinations on the renormalized lattice.

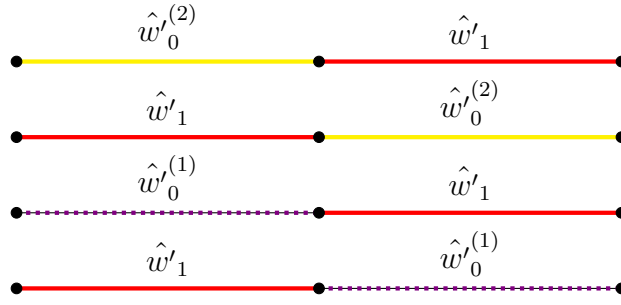


Figure 14: Image of all potential configurations involving activated and deactivated bonds. The activated bond is denoted by a red (black) line, while deactivated bonds are differentiated by color: yellow (white) for type (1) and violet (dotted) for type (2).

Similar to the initial renormalization step, the area to blocking in the subsequent step is also triangular. However, the presence of two types of deactivated bonds introduces a broader array of combinations of kernels and Ising bonds within the blocking triangles. When $A = 0$, the blocking triangles could manifest themselves in four distinct combinations during the first renormalization step. In contrast, the second step accommodates six different combinations, because of the two types of deactivated bonds. Each configuration and its corresponding weight are shown in Figure 15.

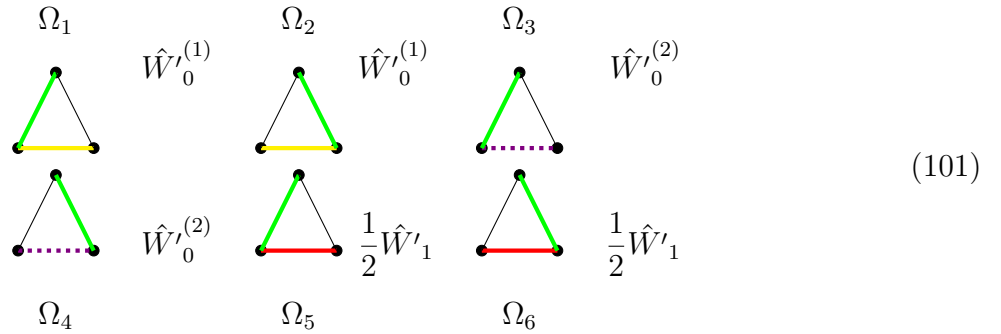


Figure 15: Boltzmann weights for all possible configurations $\Omega_{1\dots 6}$ within a blocking area, considering both activated and deactivated bonds, during the second renormalization step. The green (grey) lines indicate the kernel bonds. Yellow (white) and violet (dotted) lines represent deactivated bonds of types (1) and (2), respectively, while the red (black) line signifies an activated bond.

Given that $A = 0$, the Boltzmann weight for kernel-bonds is assigned a value of $\frac{1}{2}$. It is crucial to incorporate the factor $2^{\frac{1}{2}n_c-1}$, where n_c signifies the number of clusters within the blocking triangle. One factor of 2 is omitted as it is already accounted for in eq.(18) for the computation of the partition function. In alignment with the approach adopted in the initial renormalization step, the transfer matrix method is employed to determine the new Boltzmann weights during the second renormalization step. As shown in Figure 15, there exist six distinct blocking triangle weights, resulting in 6×6 possible combinations of two adjacent triangles. Consequently, this yields a 6×6 transfer matrix. The transfer matrix M'_b , corresponding to an

activated bond on the second renormalized lattice L'' and derived from the combination of two triangle blocking areas that result in a bond, is structured as follows:

$$M'_b = \begin{pmatrix} 0 & 0 & 0 & 0 & 0 & 0 \\ e^{-J} & 0 & \sqrt{e^{-J}}\sqrt{\sinh J} & \sqrt{e^{-J}}\sqrt{\sinh J} & 0 & 0 \\ \sqrt{e^{-J}}\sqrt{\sinh J} & 0 & \sinh J & \sinh J & 0 & 0 \\ \sqrt{e^{-J}}\sqrt{\sinh J} & 0 & \sinh J & \sinh J & 0 & 0 \\ 0 & 0 & 0 & 0 & 0 & 0 \\ 0 & 0 & 0 & 0 & 0 & 0 \end{pmatrix} \quad (102)$$

To compute the matrix W''_1 , which contains the Boltzmann weights for all conceivable configurations of an activated bond on the lattice L'' , it is necessary to multiply the matrix M'_b by the scalar weight \hat{W}'_1 of an activated bond linking two blocking triangles on the lattice L' . Additionally, the weights $\hat{W}'[B \rightarrow NB^{(1),(2)}]$ and $\hat{W}'[NB^{(1),(2)} \rightarrow B]$ from eqs.(97) and (98), which are needed when an activated bond transitions to a deactivated bond or vice versa, must also be considered. With these considerations, the Boltzmann weight of an activated bond on the lattice L'' , originating from two triangular blocking areas $W''_1[\Omega_i, \Omega_j]$, can be calculated as follows:

$$W''_1[\Omega_i, \Omega_j] = \hat{W}'_1 M'_{bij} \hat{W}'[\Omega_i \rightarrow B] \hat{W}'[B \rightarrow \Omega_j]. \quad (103)$$

Here, M'_{bij} represents the (i, j) element of the transformation matrix, and $\hat{W}'[\Omega_i \rightarrow B]$ and $\hat{W}'[B \rightarrow \Omega_j]$ are the weights mentioned earlier for scenarios where an activated bond interfaces with a deactivated bond as described in eqs. (97) and (98). It should be noted that, if an activated bond within a blocking area were to connect with another activated bond between two blocking areas, such as $\hat{W}'[\Omega_5 \rightarrow B]$, this weight would be assigned a value of one, $\hat{W}'[\Omega_5 \rightarrow B] = 1$. The transfer matrix M'_{nb} , which contains all potential configurations where no bond is activated on the lattice L'' if a bond between two blocking triangles is active, is defined as follows:

$$M'_{nb} = \begin{pmatrix} e^{-J} & e^{-J} & \sqrt{e^{-J}}\sqrt{\sinh J} & \sqrt{e^{-J}}\sqrt{\sinh J} & 0 & 0 \\ 0 & e^{-J} & 0 & 0 & 0 & 0 \\ 0 & \sqrt{e^{-J}}\sqrt{\sinh J} & 0 & 0 & 0 & 0 \\ 0 & \sqrt{e^{-J}}\sqrt{\sinh J} & 0 & 0 & 0 & 0 \\ 0 & 0 & 0 & 0 & 0 & 0 \\ 0 & 0 & 0 & 0 & 0 & 0 \end{pmatrix} \quad (104)$$

Given the constraint that a deactivated bond can only interface with another deactivated bond of the same type, it becomes necessary to introduce two additional transfer matrices. The transfer matrix $M'^{(1)}_{nb}$ is defined for scenarios where a deactivated bond of type (1) connects two blocking areas:

$$M'^{(1)}_{nb} = \begin{pmatrix} e^{-J} & e^{-J} & 0 & 0 & 0 & 0 \\ e^{-J} & e^{-J} & 0 & 0 & 0 & 0 \\ 0 & 0 & 0 & 0 & 0 & 0 \\ 0 & 0 & 0 & 0 & 0 & 0 \\ 0 & 0 & 0 & 0 & 0 & 0 \\ 0 & 0 & 0 & 0 & 0 & 0 \end{pmatrix} \quad (105)$$

Similarly, the transfer matrix $M'_{nb}{}^{(2)}$ is introduced to account for situations where a deactivated bond of type (2) connects two blocking areas. This distinction between the two types of deactivated bonds is crucial for accurately modeling the interactions within the renormalized lattice L'' .

$$M'_{nb}{}^{(2)} = \begin{pmatrix} 0 & 0 & 0 & 0 & 0 & 0 \\ 0 & 0 & 0 & 0 & 0 & 0 \\ 0 & 0 & \sinh J & \sinh J & 0 & 0 \\ 0 & 0 & \sinh J & \sinh J & 0 & 0 \\ 0 & 0 & 0 & 0 & 0 & 0 \\ 0 & 0 & 0 & 0 & 0 & 0 \end{pmatrix} \quad (106)$$

To determine the entries $W''_0[\Omega_i, \Omega_j]$ of the matrix W''_0 , which contains the Boltzmann weights for all combinations contributing to a deactivated bond between two spins on the lattice L'' , the calculation can be performed as follows:

$$\begin{aligned} W''_0[\Omega_i, \Omega_j] &= \frac{1}{2} \hat{W}'_1 M'_{nb_{ij}} \hat{W}'[\Omega_i \rightarrow B] \hat{W}'[B \rightarrow \Omega_j] \\ &\quad + \hat{W}'_0{}^{(1)} M'_{nb_{ij}}{}^{(1)} \hat{W}'[\Omega_i \rightarrow NB^{(1)}] \hat{W}'[NB^{(1)} \rightarrow \Omega_j] \\ &\quad + \hat{W}'_0{}^{(2)} M'_{nb_{ij}}{}^{(2)} \hat{W}'[\Omega_i \rightarrow NB^{(2)}] \hat{W}'[NB^{(2)} \rightarrow \Omega_j]. \end{aligned} \quad (107)$$

By diagonalizing the matrix $S'_1 W''_1 S'^{-1}_1 = D'_1$, it is observed that the matrix for the activated bonds once again has a single non-zero eigenvalue. This indicates the feasibility of extracting scalar Boltzmann weights for an activated bond directly from D'_1 . Conversely, examining the matrix W''_0 reveals that it possesses three non-zero eigenvalues, implying the existence of three types of deactivated bonds on the lattice L'' , as opposed to the two types encountered on the lattice L' . Consequently, it becomes necessary to derive three scalar Boltzmann weights from the configurations where an activated bond is connected to a deactivated bond, as represented by $S'_1 W''_1 S'^{-1}_1 S'_0 W''_0 S'^{-1}_0$, and vice versa for the scenarios where a deactivated bond connects to an activated bond. This realization underscores the potential for iterative application of the cluster-inspired renormalization group technique, albeit with a caution: each iteration increases the complexity of the method. Specifically, the transfer matrix requisite for conducting the third renormalization step would expand to an 8×8 matrix, thereby escalating the computational effort. Due to this increase in complexity, further iterations beyond this point are deemed impractical and are thus not pursued.

6 Parametrization of the Two-Dimensional Fixed Point Hamilton Function.

The cluster-inspired renormalization group transformation aggregates parallel spins into a cluster. This characteristic facilitates the possibility that, after several renormalization iterations, spins that are not immediate neighbors may be within the same cluster, thereby introducing interactions beyond nearest-neighbor interactions. Consequently, it is logical to parameterize the Hamiltonian fixed point in accordance with this observation. To achieve this, we introduce a graph ζ , representing a collection of proximal spins on the lattice. All graphs, along with their translations, reflections, and rotations, are categorized within the same equivalence class $\zeta \in \hat{\zeta}$. This classification implies that lattices exhibiting high symmetry are preferable, as a greater number of graphs will be grouped into the same equivalence class, enhancing the simplification of the model. In light of this, a triangular lattice, characterized by a 60-degree rotational symmetry, is selected for subsequent discussion. We then define a delta function $\delta_\zeta[s]$, which assumes a value of one if all spins s_ζ on the graph ζ are aligned (parallel), and zero otherwise.

$$\delta_\zeta[s] = \begin{cases} 1, & \text{if } s_x = s_\zeta, x \in \zeta, s_\zeta = \pm 1 \\ 0, & \text{otherwise.} \end{cases} \quad (108)$$

So that the fixed point Hamiltonian can be parameterised as

$$e^{-\beta\mathcal{H}^*} = \prod_{\hat{\zeta}} \prod_{\zeta \in \hat{\zeta}} W_{\hat{\zeta}}^{\delta_\zeta[s]} \quad (109)$$

Where $W_{\hat{\zeta}}$ represents the Boltzmann weights corresponding to the graphs within the equivalence class $\hat{\zeta}$. Additionally, it is observed that the Boltzmann weight is not one ($W_{\hat{\zeta}} \neq 1$) if and only if all spins on the graph are aligned, as indicated by the condition $\delta_\zeta[s] = 1$. An example of a graph is presented in figure 16.

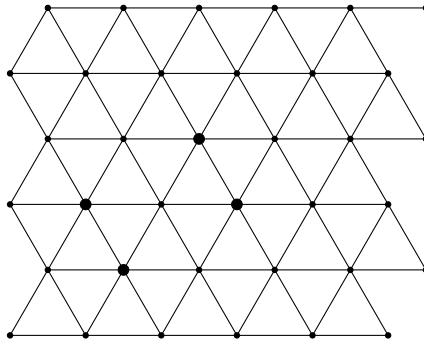
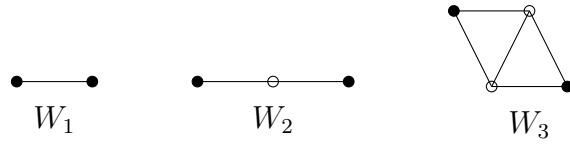
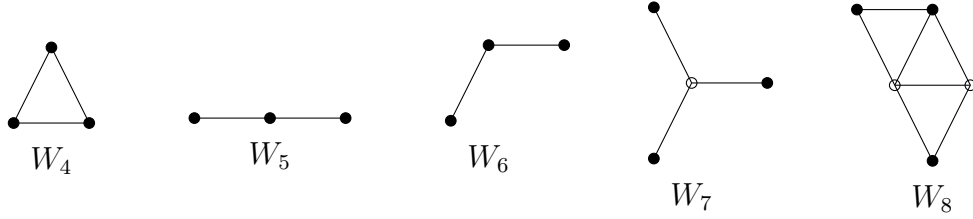


Figure 16: The graph W_{13} is activated with four parallel spins, represented by four bold black points.

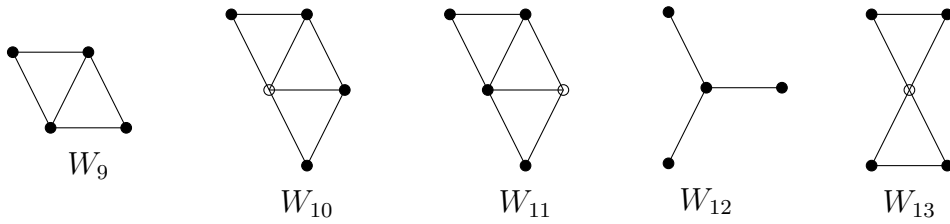
For practical reasons, the graphs must be restricted to a feasible number of spins. Given that the fixed point Hamiltonian is presumed to be local, this constraint does not impose significant limitations due to the diminished contribution of graphs containing a larger number of spins to the overall weight of a spin configuration and, consequently, to the partition function of the system. Hence, for all considered graphs, the separation between spins is restricted to no more than two lattice spacing. On the triangular lattice, the two-point graphs have the following geometry:



Similarly, the three-point graphs considered within the constraint of a maximum relative distance of two lattice spacings between spins are:



Likewise, for the four-point graphs:



Adopting the same approach, the scope could be extended to include 5-point, 6-point, or even larger graphs. It is crucial to recognize that imposing a limit on the size of the graphs effectively truncates the fixed point Hamiltonian. By incorporating higher-order n -point functions, the approximation of the fixed point progressively improves.

7 Finite-Volume Approximation of the Fixed Point

Given that the fixed point Hamiltonian is inherently local, its finite-volume approximations yield significant insights into the characteristics of the fixed point Hamiltonian within an infinitely extensive lattice framework. The triangular lattice, characterized by its hexagonal symmetry (a 60-degree rotational invariance), is particularly well-suited for finite-volume analysis due to this high rotation symmetry.

For this study, a finite lattice configured in a hexagonal shape with periodic boundary conditions was employed. This lattice configuration comprises 12 Ising spins on a finer lattice, which, through a blocking transformation characterized by a blocking factor of $\sqrt{3}$, coarsens into a lattice with 4 Ising spins. This transformation and the resulting lattice structure are shown in Figure 17.

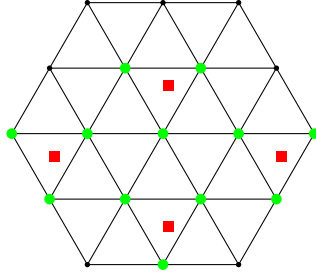


Figure 17: Finite hexagon-shaped lattice with periodic boundary conditions. Twelve fine spins (green (grey) dots) were put on the lattice. After one renormalization step with factor $\sqrt{3}$ blocking, three spins are blocked together to one coarse spin (red rectangle).

The implementation of periodic boundary conditions is such that the upper-left edge of the hexagon corresponds periodically to the lower-right edge, the upper-right edge to the lower-left, and the upper horizontal edge to the lower horizontal edge. These boundary conditions enable the construction of an extended lattice by lining up multiple hexagonal units.

To analytically derive the equations defining the fixed point Hamiltonian, as specified in eq. (109), it is necessary to enumerate all possible spin configurations on the coarse lattice. Given the \mathbb{Z}_2 symmetry intrinsic to the Ising model, the distinct configurations include those where all spins are aligned, three spins are aligned with one opposing, and configurations with an equal number of up and down spins. These considerations lead to the following conditions:

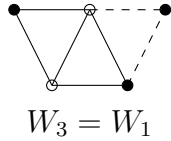
$$\begin{aligned}
 e^{-\beta\mathcal{H}_1} &= e^{-\beta h(\uparrow,\uparrow,\uparrow,\uparrow)} \\
 e^{-\beta\mathcal{H}_2} &= e^{-\beta h(\downarrow,\uparrow,\uparrow,\uparrow)} \\
 e^{-\beta\mathcal{H}_3} &= e^{-\beta h(\downarrow,\downarrow,\uparrow,\uparrow)}
 \end{aligned} \tag{110}$$

Here, $e^{-\beta\mathcal{H}_1}$ represents the configurations on the finer lattice that, after one renormalization step, lead to the coarse lattice configuration where all spins are aligned upwards, denoted by $e^{-\beta h(\uparrow,\uparrow,\uparrow,\uparrow)}$. The terms $e^{-\beta\mathcal{H}_2}$ and $e^{-\beta\mathcal{H}_3}$ are defined analogously for their respective configurations.

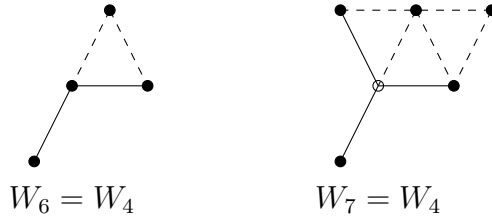
To compute the Boltzmann weights for the fine configurations that correspond to one of the three distinct configurations on the coarse lattice, it's necessary to account for all $2^{12} = 4096$ configurations on the fine lattice. This task is feasible using a standard computer. However, the next larger hexagon-shaped lattice in our framework would consist of 27 fine spins, leading to

$2^{27} = 134,217,728$ configurations. Evaluating such a vast number of configurations exceeds the capabilities of an average computer available for carrying out the calculations for this thesis.

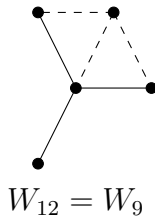
The truncation of the fixed point Hamiltonian function is characterized by various n -point graphs as discussed in Chapter 6. Therefore, one must evaluate all possible combinations of n -point graph Boltzmann weights $e^{-\beta\mathcal{H}}$ for a given fine lattice spin configuration, which results in a corresponding combination of n -point graphs on the coarse lattice $e^{-\beta h}$. This necessitates distinguishing between the n -point graphs on the coarse lattice. Due to the periodicity of the fine lattice under shifts by $2\sqrt{3}a$ in directions orthogonal to the hexagon edges, the coarse lattice exhibits periodicity under shifts by $2a'$, where $a' = \sqrt{3}a$. Among all 2-point graphs, only the W_1 graph needs to be considered, as the others are indistinguishable from it within this context. The W_2 graph does not qualify as a true 2-point graph since, under the $2a'$ periodicity, it decomposes into a 1-point graph. Likewise, the W_3 graph cannot be distinguished from W_1 .



The 3-point graphs W_5 and W_8 decomposes into 2-point graphs. The graphs W_6 and W_7 can not be distinguished from W_4 because of the periodicity of translation shifts by $2a'$.



In the analysis of 4-point graphs, only W_9 requires consideration. This is because W_{10} and W_{11} decompose into 3-point graphs, while W_{13} reduces to a 2-point graph. Furthermore, W_{12} is found to be in the same equivalence class as W_9 when considering shifts of $2a'$, making it redundant for separate analysis. This selection process is pivotal for simplifying the computational workload, ensuring that only the most representative and non-redundant graphs are evaluated to characterize the fixed point Hamiltonian effectively.



Given that there are only 4 coarse spins, the consideration of n -point graphs is limited to those with n no greater than 4. Consequently, the Boltzmann weights of the fine lattice configurations denoted as $e^{-\beta\mathcal{H}}$, and those on the coarse lattice, represented by $e^{-\beta h}$, can be effectively described as functions of the graph weights W_1 , W_4 , and W_9 only.

It is important to recognize that the hexagonal periodicity inherent to the lattice structure is, in essence, equivalent to parallelogram periodicity. This observation simplifies the calculation of Boltzmann weights by allowing the use of a more straightforward geometric representation without losing the essential topological characteristics of the hexagonal lattice.

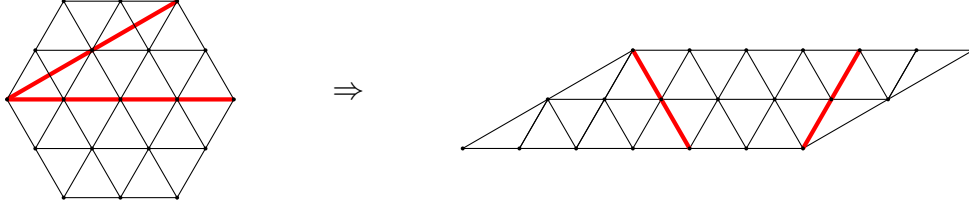


Figure 18: The hexagonal-shaped lattice can be cut along the thick red(black) lines and re-assembled into an equivalent parallelogram-shaped lattice.

This inherent property substantially simplifies the enumeration of spins, thereby improving the identification of nearest-neighbors for each spin. Moreover, defining the blocking areas is more straightforward in a lattice with a parallelogram geometry. Consequently, the hexagonal-shaped lattice shown in figure 17 can be effectively reformulated as an equivalent parallelogram-shaped lattice, as illustrated in figure 19.

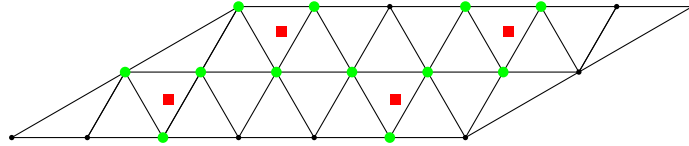


Figure 19: Finite volume lattice in parallelogram-shape. This lattice is equivalent to the hexagon-shaped lattice of figure 17.

It is crucial to recognize that the blocking kernel breaks the 30° rotational symmetry of the lattice, reducing it to a 120° symmetry. This arises from the orientation of the blocking area, which can be either a downward oriented triangle, as illustrated in Figure 17, or upward oriented. Post-blocking, the resultant lattice regains a 30° rotational symmetry. The transformation from a fine to a coarse configuration employs the blocking kernel $T(s_x; x \in \Omega_{x'}, s'_{x'}) = A + \frac{1-2A}{N} \sum_{x \in \Omega_{x'}} \delta_{s_x, s'_{x'}}$, initially introduced in eq.(75).

The contribution of the blocking kernel to the total Boltzmann weight of a coarse configuration depends on the spin arrangement, as delineated by the following values:

$$\begin{aligned}
 T(\uparrow\uparrow\uparrow, \uparrow) &= A + \left(\frac{1-2A}{3}\right) 3 = 1 - A \\
 T(\uparrow\uparrow\uparrow, \downarrow) &= A + \left(\frac{1-2A}{3}\right) 0 = A \\
 T(\uparrow\uparrow\downarrow, \uparrow) &= A + \left(\frac{1-2A}{3}\right) 2 = \frac{2}{3} - \frac{A}{3} \\
 T(\uparrow\uparrow\downarrow, \downarrow) &= A + \left(\frac{1-2A}{3}\right) 1 = \frac{1}{3} + \frac{A}{3}
 \end{aligned} \tag{111}$$

The central arrow in the shown triangles signifies the coarse spin resultant from the blocking process. The factor a fine lattice configuration acquires from the blocking kernel is expressed as:

$$A^{n_0} \left(\frac{1}{3} - \frac{A}{3}\right)^{n_1} \left(\frac{2}{3} - \frac{A}{3}\right)^{n_2} (1 - A)^{n_3}$$

where $n_i, i = 0, 1, 2, 3$ denotes the number of blocks with i fine spins matching the new coarse spin.

The Boltzmann weight of a given configuration, parameterized by the n -point graph weights W_1, W_4 , and W_9 , following a renormalization step, is:

$$e^{-\beta\mathcal{H}_{\text{conf.}}} = A^{n_0} \left(\frac{1}{3} - \frac{A}{3}\right)^{n_1} \left(\frac{2}{3} - \frac{A}{3}\right)^{n_2} (1 - A)^{n_3} W_1^{m_1} W_4^{m_4} W_9^{m_9}, \tag{112}$$

where $m_j, j = 1, 4, 9$ represents the number of occurrence for the graphs W_j on the fine spin configuration.

The same n -point graphs define the Boltzmann weights on the coarse lattice $e^{-\beta h}$, yet only three distinct Boltzmann weights emerge due to the coarse lattice's four-spin configuration:

$$\begin{aligned}
 e^{-\beta h(\uparrow, \uparrow, \uparrow, \uparrow)} &= 2^8 W_1'^{12} W_4'^8 W_9'^{12} \\
 e^{-\beta h(\uparrow, \uparrow, \uparrow, \downarrow)} &= 2^8 W_1'^6 W_4'^2 \\
 e^{-\beta h(\uparrow, \uparrow, \downarrow, \downarrow)} &= 2^8 W_1'^4
 \end{aligned} \tag{113}$$

To ensure consistency between the partition functions expressed in terms of the graph weights W_i and their transformed counterparts W'_i , a factor of 2^8 has to be included. This adjustment

is crucial in scenarios where all graph weights are one, ensuring that the partition functions remain equivalent under such conditions. The mathematical representation of this equivalence is given by:

$$Z(W_1, W_4, W_9) = 2^{12} \quad \text{if} \quad W_i = 1, i = 2, 4, 9 \quad (114)$$

$$Z(W'_1, W'_4, W'_9) = 2^8 2^4 = 2^{12} \quad \text{if} \quad W'_i = 1, i = 2, 4, 9 \quad (115)$$

It is important to note that the inclusion of this factor is necessary solely due to the finite-volume framework of the analysis. In the infinite volume limit, where the lattice size approaches infinity, the necessity to include such a factor disappears; the lattice, despite being coarsened, remains infinite, and the partition functions inherently align without the need for additional adjustments.

The process of determining the fixed point condition equations involves anchoring the spin values on the coarser lattice and subsequently computing the weights for all fine lattice configurations that correspond to the given coarse configuration, as defined by eq. (112). With this approach the fixed point conditions of eq.(110) can be determined. Note that for the following discussion the factor A of the blocking kernel is set to zero $A = 0$.

In the particular scenario where all spins on the coarse lattice are aligned, the corresponding equation can be expressed as follows:

$$\begin{aligned} & \frac{W_1^{12}}{3^4} (555 + (W_1 W_4)^2 (1080 + 852 W_9) + (W_1 W_4)^4 (1188 + 384 W_9 + 762 W_9^2 + 1512 W_9^3) \\ & + (W_1 W_4)^6 (96 + 240 W_9^2 + 72 W_9^3 + 1728 W_9^4 + 1296 W_9^5 + 648 W_9^6) \\ & + (W_1 W_4)^8 (48 W_9^4 + 2232 W_9^6 + 606 W_9^8 + 1584 W_9^7) + (W_1 W_4)^{10} (288 W_9^9 + 720 W_9^{10} + 1440 W_9^{11}) \\ & + (W_1 W_4)^{12} (840 W_9^{12} + 648 W_9^{14}) + 1188 (W_1 W_4)^{14} W_9^{17} + 648 (W_1 W_4)^{18} W_9^{24} \\ & + 81 (W_1 W_4)^{24} W_9^{36}) = 2^8 W_1^{12} W_4^8 W_9^{12}. \end{aligned} \quad (116)$$

The equation when three spins are parallel and one is anti-parallel reads:

$$\begin{aligned} & \frac{W_1^{12}}{3^4} (606 + (W_1 W_4)^2 (1458 + 1092 W_9) + (W_1 W_4)^4 (1458 + 696 W_9 + 912 W_9^2 + 1458 W_9^3) \\ & + (W_1 W_4)^6 (39 + 327 W_9^2 + 252 W_9^3 + 3618 W_9^4 + 1134 W_9^5 + 486 W_9^6) \\ & + (W_1 W_4)^8 (60 W_9^4 + 3276 W_9^6 + 738 W_9^7 + 528 W_9^8) + (W_1 W_4)^{10} (414 W_9^9 + 387 W_9^{10} + 774 W_9^{11}) \\ & + (W_1 W_4)^{12} (402 W_9^{12} + 162 W_9^{14}) + 378 (W_1 W_4)^{14} W_9^{17} + 81 (W_1 W_4)^{18} W_9^{24}) = 2^8 W_1^6 W_4^2. \end{aligned} \quad (117)$$

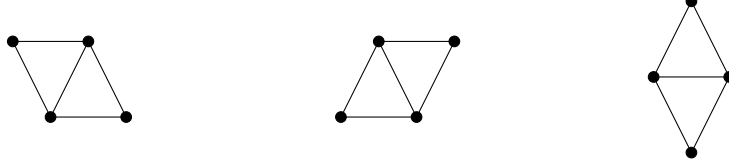
In scenarios where two spins on the coarse lattice differ from the other two, the equation is expressed as:

$$\begin{aligned} & \frac{W_1^{12}}{3^4} (627 + (W_1 W_4)^2 (1584 + 1176 W_9) + (W_1 W_4)^4 (1548 + 888 W_9 + 960 W_9^2 + 1440 W_9^3) \\ & + (W_1 W_4)^6 (24 + 456 W_9^2 + 288 W_9^3 + 4320 W_9^4 + 972 W_9^5 + 432 W_9^6) \\ & + (W_1 W_4)^8 (147 W_9^4 + 3636 W_9^6 + 432 W_9^7 + 552 W_9^8) + (W_1 W_4)^{10} (324 W_9^9 + 216 W_9^{10} + 432 W_9^{11}) \\ & + (W_1 W_4)^{12} (156 W_9^{12} + 54 W_9^{14}) + 72 (W_1 W_4)^{14} W_9^{17}) = 2^8 W_1^4. \end{aligned} \quad (118)$$

This results in a highly non-linear system of equations. A further consideration would be to use the 4-point graph W_{12} instead of W_9 . This is because the equivalence class of W_{12} contains two graphs.



In comparison with the W_9 graphs, which contain three different graphs in their equivalence class.



Because of this, the W_{12} graph has higher symmetry and may be preferred by the system. The system of equations referred to in eq.(110), considering the W_{12} graph instead of W_9 , reads:

$$\begin{aligned}
 & \frac{W_1^{12}}{3^4} (24 + 96W_{12}^2 + 144W_{12}^4 + 240W_{12}^5 + 51W_{12}^8 + (W_1W_4)^2(1080 + 624W_{12}^3 + 228W_{12}^4) \\
 & + (W_1W_4)^4(1188 + 384W_{12} + 504W_{12}^2 + 786W_{12}^4 + 984W_{12}^5) \\
 & + (W_1W_4)^6(168 + 816W_{12} + 936W_{12}^2 + 264W_{12}^3 + 1320W_{12}^4 + 288W_{12}^7 + 288W_{12}^{10}) \\
 & + (W_1W_4)^8(144 + 384W_{12} + 660W_{12}^2 + 1488W_{12}^3 + 210W_{12}^4 + 1584W_{12}^6) \\
 & + (W_1W_4)^{10}(1008W_{12}^4 + 1440W_{12}^7) + (W_1W_4)^{12}(408W_{12}^6 + 432W_{12}^8 + 648W_{12}^{12}) \\
 & + (W_1W_4)^{14}(1188W_{12}^{10}) + 648(W_1W_4)^{18}W_{12}^{16} + 81(W_1W_4)^{24}W_{12}^{24} = 2^8 W_1'^{12} W_4'^8 W_{12}'^8
 \end{aligned}$$

$$\begin{aligned}
 & \frac{W_1^{12}}{3^4} (30 + 120W_{12}^2 + 180W_{12}^4 + 246W_{12}^5 + 30W_{12}^8 + (W_1W_4)^2(1458 + 726W_{12}^3 + 366W_{12}^4) \\
 & + (W_1W_4)^4(1458 + 696W_{12} + 738W_{12}^2 + 888W_{12}^4 + 744W_{12}^5) \\
 & + (W_1W_4)^6(291 + 1452W_{12} + 1413W_{12}^2 + 708W_{12}^3 + 1623W_{12}^4 + 252W_{12}^7 + 117W_{12}^{10}) \\
 & + (W_1W_4)^8(396 + 642W_{12} + 1122W_{12}^2 + 1536W_{12}^3 + 168W_{12}^4 + 738W_{12}^6) \\
 & + (W_1W_4)^{10}(801 + 774W_{12}^7) + (W_1W_4)^{12}(294W_{12}^6 + 108W_{12}^8 + 162W_{12}^{12}) + 378(W_1W_4)^{14}W_{12}^{10} \\
 & + 81(W_1W_4)^{18}W_{12}^{16} = 2^8 W_1'^6 W_4'^2
 \end{aligned}$$

$$\begin{aligned}
 & \frac{W_1^{12}}{3^4} (33 + 132W_{12}^2 + 198W_{12}^4 + 240W_{12}^5 + 24W_{12}^8 + (W_1W_4)^2(1584 + 768W_{12}^3 + 408W_{12}^4) \\
 & + (W_1W_4)^4(1548 + 888W_{12} + 792W_{12}^2 + 984W_{12}^4 + 624W_{12}^5) \\
 & + (W_1W_4)^6(312 + 1680W_{12} + 1692W_{12}^2 + 912W_{12}^3 + 1608W_{12}^4 + 216W_{12}^7 + 72W_{12}^{10}) \\
 & + (W_1W_4)^8(639 + 960W_{12} + 1200W_{12}^2 + 1344W_{12}^3 + 192W_{12}^4 + 432W_{12}^6) \\
 & + (W_1W_4)^{10}(540W_{12}^4 + 432W_{12}^7) + (W_1W_4)^{12}(120W_{12}^6 + 36W_{12}^8 + 54W_{12}^{12}) \\
 & + 72(W_1W_4)^{14}W_{12}^{10} = 2^8 W_1'^4
 \end{aligned} \tag{119}$$

In the analysis of W_9 , no non-trivial solutions with positive weights were identified, except for the trivial case where all weights are one. For W_{12} , beyond the trivial fixed point, a solution given by $W_1 = 0.232335$, $W_4 = 27.7693$, $W_{12} = 0.132717$ was discovered. However, this solution presents a challenge, as the value of W_1 is less than one, which is inconsistent with ferromagnetic behavior. These findings suggest that the chosen finite volume consideration may be insufficient to accurately approximate the fixed point. This limitation might stem from the renormalized lattice configuration, which comprises only four spins arranged with a periodicity of two lattice spacings. This setup raises uncertainties regarding the possible number of distinct graphs that can be accommodated, given that different graphs may share spins but differ in the links connecting the spins.

8 Conclusion

After a brief introduction to the Ising model and its properties, followed by an introduction to the renormalization group and its characteristics, a general overview of the renormalization of the Ising model is provided. Then in Chapter 5, the Ising model was subject to renormalization via the renormalization group decimation technique. This approach yielded two central equations: one describing the evolution of the nearest-neighbor interaction coupling, and the other characterizing the magnetic field's behavior. These equations elucidate the trajectory of the couplings across renormalization steps. Subsequently, the renormalization group blocking method was employed to devise a blocking scheme in the presence of an external magnetic field. The selected blocking kernel was formulated to permit the orientation of the renormalized spins not to align with the original spins within the blocking domain. This framework enabled the determination of the coupling flows at each renormalization stage, demonstrating a consistent halving of the correlation length after each iteration.

Following the exploration of the established renormalization group decimation and blocking techniques, a novel cluster-inspired renormalization scheme for the Ising model, expressed in the cluster representation, was developed. Using the transfer matrix method, it was possible to compute matrices encapsulating the Boltzmann weights associated with both activated and deactivated bonds in the renormalized system. This led to the formulation of new scalar Boltzmann weights, distinct for activated bonds and two types of deactivated bonds, facilitating the reconstruction of a local cluster representation Hamiltonian for the renormalized lattice. This approach allowed to determine the change of the original Boltzmann weights transforming under the chosen blocking kernel. Additionally, a method was devised to iteratively apply the renormalization process, successfully executing one iteration. However, it was observed that the complexity of the system escalated with each renormalization step. This escalation is attributed to the increasing number of eigenvalues corresponding to the deactivated bond matrix, which, in turn, results in a diversification of deactivated bond types. Consequently, also increasing the number of scalar Boltzmann weights.

In Chapter 6, a method for the parametrization of the two-dimensional fixed point was established. Assuming the fixed point Hamiltonian to be local and the decay of long-distance interactions to be exponential, a strategy was devised to parametrize the Hamiltonian of the fixed-point using n -point graphs. This approach yielded a sufficient variety of unique graphs, not confined to the same equivalence class, thus facilitating a finite-volume approximation of the fixed point on a triangular lattice, as further detailed in Chapter 7. The computation of the blocking kernel weights and the selection of a set of indistinguishable n -point graphs on the finite lattice led to the formulation of a system of highly nonlinear equations governing the fixed point Boltzmann weights. These equations allowed for the identification of the trivial fixed point.

Future work may extend the one-dimensional cluster-inspired blocking to two dimensions, examining its impact on the model's iterative dynamics and the potential increase of the number of different bond types. Additionally, the effect of employing larger starting lattices on the finite-volume approximation of the fixed point warrants investigation. The current study utilized a fine lattice comprising 12 spins, resulting in a coarse lattice with 4 spins after factor $\sqrt{3}$ blocking. The high translational symmetry observed due to the limited spin count on the fine lattice led to the decomposition of many n -point functions. Exploring scenarios with larger fine lattices could diminish finite-volume effects and provide new insights. For instance, the

next smaller hexagon-shaped lattice contains 9 coarse spins, scaling to a fine lattice with 27 spins, presenting $134'217'728$ possible spin configurations, rendering analytical computation of condition equations infeasible. Thus, numerical techniques, such as Monte Carlo methods, may prove essential for deeper insights into the approximate fixed point Hamiltonian, with the analytical cases serving as benchmarks for validating the correctness of the selected Monte Carlo algorithms.

References

- [1] E. Ising. *Beitrag zur Theorie des Ferro-und Paramagnetismus*. PhD thesis, Grefe & Tiedemann Hamburg, Germany, 1924.
- [2] L. Onsager. Crystal statistics. i. a two-dimensional model with an order-disorder transition. *Phys. Rev.*, 65:117–149, Feb 1944.
- [3] R.J. Baxter. *Exactly Solved Models in Statistical Mechanics*. Academic Press London, 1982.
- [4] K. G. Wilson. Renormalization group and critical phenomena. i. renormalization group and the kadanoff scaling picture. *Phys. Rev. B*, 4:3174–3183, Nov 1971.
- [5] K. G. Wilson. The renormalization group: Critical phenomena and the kondo problem. *Rev. Mod. Phys.*, 47:773–840, Oct 1975.
- [6] G. Mussardo. *Statistical Field Theory*. Oxford University Press, 2015.
- [7] M. Nauenberg. Renormalization group solution of the onedimensional Ising model. *Journal of Mathematical Physics*, 16(3):703–705, 03 1975.
- [8] L. Kadanoff. *Statistical physics: statics, dynamics and renormalization*. World Scientific, 2000.
- [9] U.-J. Wiese. *Statistical Mechanics*. Institute for Theoretical Physics, Bern University, 2010.
- [10] M.E.J. Newman and G.T.Barkema. *Monte Carlo Methods in Statistical Physics*. Oxford University Press, 1999.
- [11] J.-S. Wang and R. H. Swendsen. Cluster monte carlo algorithms. *Physica A: Statistical Mechanics and its Applications*, 167(3):565–579, 1990.
- [12] D. P. Landau and K. Binder. *Monte Carlo Simulations in Statistical Physics*. Cambridge University Press, 2021.
- [13] D.A Lavis and G.M.Bell. *Statistical Mechanics of Lattice Systems 2*. Springer-Verlag Berlin Heidelberg, 1999.
- [14] H. A. Farach R. J. Creswick and C. P. Poole. *Introduction to Renormalization Group Methods In Physics*. John Wiley and Sons, 1992.